RESEARCH REPORT

Decorrelation criterion to select diffusion stopping time: experimental evaluation

Pavel Mrázek

mrazekp@cmp.felk.cvut.cz

Center for Applied Cybernetics
Faculty of Electrical Engineering, Czech Technical University
Technická 2, 166 27 Praha 6, Czech Republic
www: http://cmp.felk.cvut.cz

CTU–CMP–2002–01

Published also as: K333–13/02

January 15, 2002

Contents

Abstract

In a previous work [7], we developed a novel time-selection strategy for iterative image restoration techniques. We call it *decorrelation criterion* as the stopping time is chosen so that the correlation of signal and noise in the filtered image is minimised. This research report presents a detailed experimental evaluation of this stopping criterion, running several types of filters on various images artificially corrupted with noise, and comparing the optimal values of the stopping time T with the estimates.
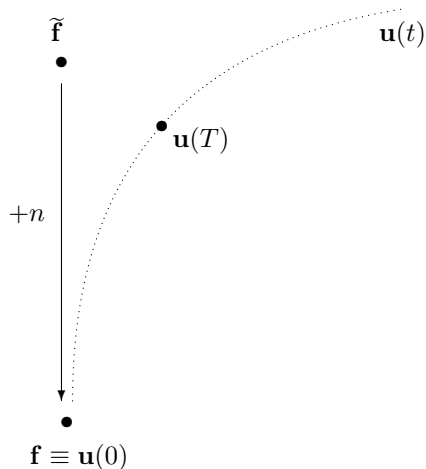
Figure 1: Model of the time-selection problem for the diffusion filtering. We want to select the filtered image $\mathbf{u}(T)$ which is as close as possible to the ideal signal $\widetilde{\mathbf{f}}$.

1 Introduction

If we want to restore noisy images using some method which starts from the input data and creates a set of possible filtered solutions by gradually removing noise and details from the data, the crucial question is when to stop the filtering in order to obtain the optimal restoration result. The choice of the stopping time T has a strong effect on the diffusion result: small T gives more trust to the input data (and leaves more details and noise in the data unfiltered), while large T means that the result becomes dominated by the model of the filtering process.

We work with the following model (see Fig. 1): let $\widetilde{\mathbf{f}}$ be an ideal, noise-free (discrete) image; this image is observed by some imprecise measurement device to obtain an image $\mathbf{f}$. We assume that some noise n is added to the signal during the observation so that

$$\mathbf{f} = \widetilde{\mathbf{f}} + n. \tag{1}$$

Furthermore, we assume that the noise n is uncorrelated with the signal $\widetilde{\mathbf{f}}$, and that the noise has zero mean value, $E(n) = 0$.

The diffusion filtering starts with the noisy image as its initial condition, $\mathbf{u}(0) = \mathbf{f}$, and the diffusion evolves along some trajectory $\mathbf{u}(t)$. This trajectory depends on the diffusion parameters and on the input image; the optimistic assumption is that the noise will be removed from the data before any important features of the signal commence to deteriorate significantly, so that the diffusion leads us somewhere 'close' to the ideal data. This should be the case if the signal adheres to the piecewise constant model inherent in the diffusion equation.

The task of the stopping time selection can be formulated as follows: select that point $\mathbf{u}(T)$ of the diffusion evolution which is nearest to the ideal signal $\widetilde{\mathbf{f}}$. Obviously, the ideal signal is normally not available; the optimal stopping time T can only be estimated by some criteria, and the distance[1] between the ideal and the filtered data serves only in the experiments to evaluate the performance of the estimation procedure.

In [7] we claimed that a near-optimal estimate of the stopping time can be often obtained if we use the formula

$$T = \arg \min_{t} \operatorname{corr}\big(\mathbf{u}(0) - \mathbf{u}(t), \mathbf{u}(t)\big). \tag{2}$$

---

[1]In the experiments below, we measure the distance of two images by the *mean absolute deviation*, $\mathrm{MAD}(x - y) = E(|x - y|)$. The MAD distance is equivalent to the l_1 norm normalized by the number of pixels; we favour it over e.g. the l_2 norm because it is less sensitive to outliers.
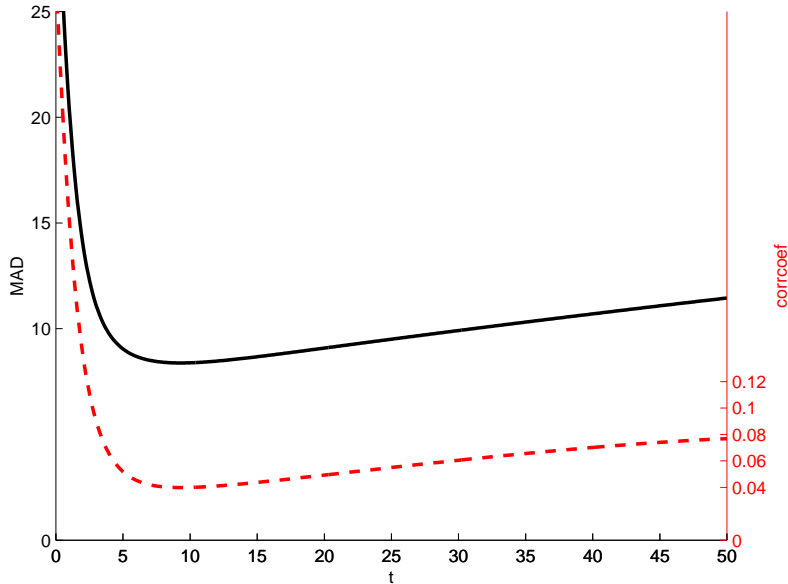
Figure 2: The distance $\mathrm{MAD}(\mathbf{u}(t) - \widetilde{\mathbf{f}})$ (solid line) and the correlation coefficient $\mathrm{corr}\big(\mathbf{u}(0) - \mathbf{u}(t), \mathbf{u}(t)\big)$ (dashed line) developing with the diffusion time. The graphs were measured experimentally on noisy cymbidium data of SNR = 6 filtered using anisotropic NL diffusion.

We call this equation the *decorrelation criterion*. In this paper, we test and evaluate its performance experimentally.

2 Experiments

In the experiments below, we simulate the image formation process sketched above by taking some image, either natural of artificially created, and declaring it to be noise-free and represent the ground truth $\widetilde{\mathbf{f}}$. Then we add some noise n to the image artificially, filter the noisy image $\mathbf{u}(0) = \widetilde{\mathbf{f}} + n$ using several methods, and observe the development of the distance between the filtered signal and the noise-free image, $\mathrm{MAD}\big(\mathbf{u}(t) - \widetilde{\mathbf{f}}\big)$, and the development of the correlation between the filtered signal $\mathbf{u}(t)$ and the 'filtering noise' $\mathbf{u}(0) - \mathbf{u}(t)$.

Ideally, the two graphs will look something like those in Fig. 2. You can see that the distance $\mathrm{MAD}\big(\mathbf{u}(t) - \widetilde{\mathbf{f}}\big)$ decreases in the first iterations as the noise is smoothed, and then starts to increase again as also the useful signal begins to disappear under the filtering process. The graph of the correlation coefficient $\mathrm{corr}\big(\mathbf{u}(0) - \mathbf{u}(t), \mathbf{u}(t)\big)$ exhibits a highly similar behaviour; this similarity lets us hope that we can estimate the stopping time T which optimises the filtering quality (measured by the MAD distance) by locating the minimum of the correlation $\mathrm{corr}\big(\mathbf{u}(0) - \mathbf{u}(t), \mathbf{u}(t)\big)$.

In our experiments, we will compare several values: T_{opt} will stand for the optimal stopping time which minimizes the distance between the filtered and the ideal data (known in the experimental setup only), and D_{opt} will denote the value of this optimal distance, $D_{\mathrm{opt}} = \mathrm{MAD}\big(\mathbf{u}(T_{\mathrm{opt}}) - \widetilde{\mathbf{f}}\big)$. The symbol T_{corr} will stand for the stopping time estimated using the decorrelation criterion (2), and D_{corr} will represent the filtering residual at such a stopping time. In some cases we also compare the results to the estimation using the method of Weickert [10] which requires knowledge of the signal-to-noise ratio (SNR) in the input image and iterates the diffusion until the filtered signal is in some distance from the noisy input; the values obtained using this method will be denoted T_{SNR} and D_{SNR}.
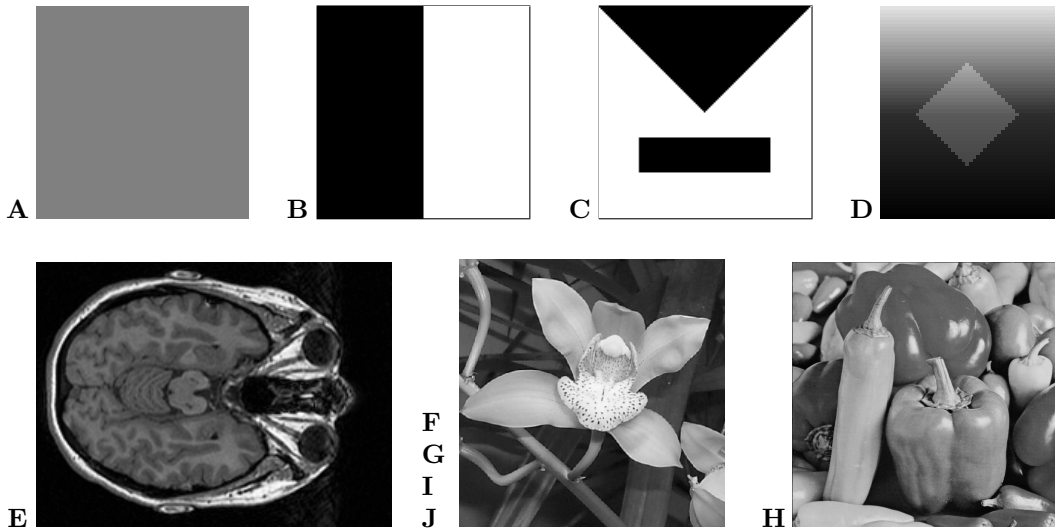
Figure 3: Original images used in experiments A–H.

The filtering methods we use include linear diffusion alias low-pass filtering [4], nonlinear (NL) diffusion [8, 2], anisotropic NL diffusion (especially its 'edge-enhancing' form [9]), monotonicity-enhancing NL diffusion[5] (see also the thesis [6] for more information on these diffusion filters), and iterated median filtering.

Linear and NL diffusion (both isotropic and anisotropic) are representatives of information-reducing scale spaces obeying e.g. the maximum-minimum principle. Although we have proved such a property for linear diffusion only, the experiments suggest that all these methods guarantee non-negativity of the correlation between filtered signal and filtering noise, $\mathrm{corr}\big(\mathbf{u}(0) - \mathbf{u}(t), \mathbf{u}(t)\big) \geq 0$. This non-negativity is not ensured by monotonicity-enhancing NL diffusion and iterated median filtering; for these two methods, we employ absolute value of the correlation in (2) to estimate the stopping time.

In this paper, we present the results of several series of experiments. In **Experiments A–H** (sections 2.2 to 2.9) we corrupt the original image with varied amount of noise[2], filter the noisy image using several filters, and compare the filtering results. We present and compare the optimal and decorrelation-estimated stopping times, T_{opt} and T_{corr}, as well as the corresponding distances between the filtered and ideal signal, D_{opt} and D_{corr}.

Experiment I (section 2.11) offers a comparison between estimations of stopping time using the decorrelation criterion and the SNR method of Weickert [10], measured on the cymbidium data with additive Gaussian noise filtered using anisotropic NL diffusion.

Experiment J (section 2.12) examines the possibility to use minimum of the signal–noise correlation to select optimal filtering method or optimal filtering parameters. The idea is that the less the filtered signal is correlated with the filtering noise, the better the filtering performance. We will test this assumption through varying the diffusivity parameter λ, and running several experiments to compare between different filters.

Last, some images filtered using the decorrelation estimaton of the stopping time are gathered for illustration in section 2.13.

D_{opt}	D_{corr}

all filters

D_{opt}	D_{corr}

anisotropic NL diffusion

$D_{\text{opt}}, D_{\text{corr}}$	$T_{\text{opt}}, T_{\text{corr}}$

linear diffusion

$D_{\text{opt}}, D_{\text{corr}}$	$T_{\text{opt}}, T_{\text{corr}}$

monotonicity-enhancing NL diff.

$D_{\text{opt}}, D_{\text{corr}}$	$T_{\text{opt}}, T_{\text{corr}}$

isotropic NL diffusion

$D_{\text{opt}}, D_{\text{corr}}$	$T_{\text{opt}}, T_{\text{corr}}$

iterated median filtering
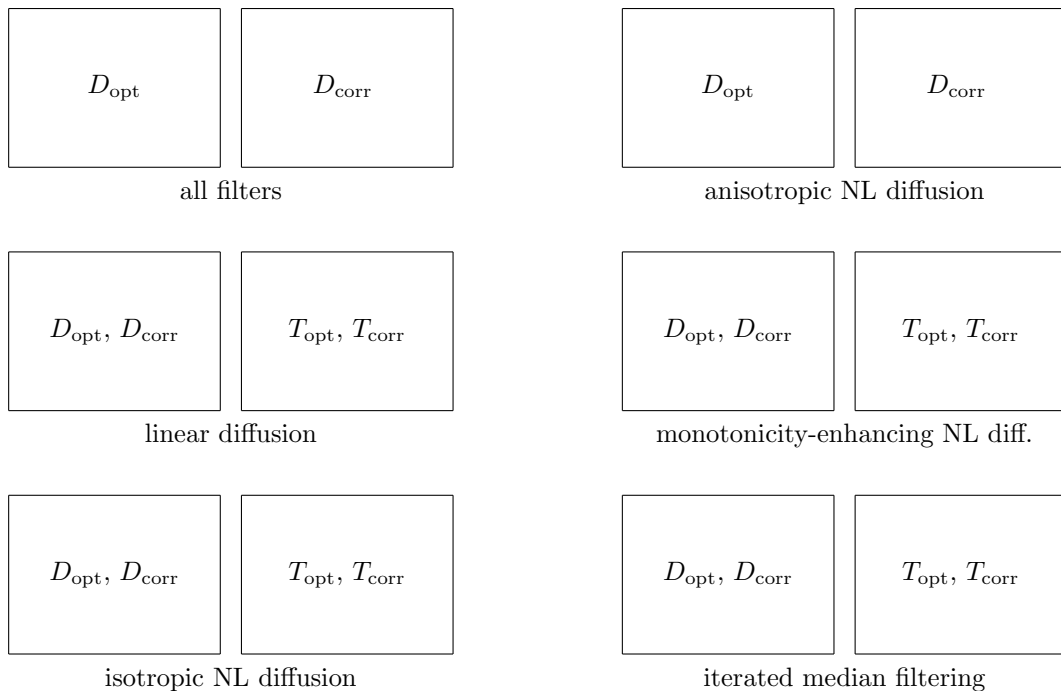
Figure 4: Layout of the presented graphs in experiments B–H.

2.1 Introduction to experiments A–H

In experiments A–H we will use several images (shown in Fig. 3), declare them to be noise-free, corrupt each of them with varied amount of noise and filter with several filters. For each image, we will then show a table which compares the optimal stopping time T_{opt} with the estimated T_{corr}, and a table comparing the distances between the original and filtered images for both stopping times, D_{opt} and D_{corr}. Then (with the exception of Experiment A), we show a series of graphs drawn using the measured values T and D, with the structure illustrated in Fig. 4. In each of these graphs, the horizontal axis represents the amount of noise in the input image, so that the intersection of one vertical line with the graphs represents the results obtained from one noisy input image using one or several filters.

---

[2]We employ Gaussian additive noise in all cases except Experiment G, where the image is corrupted with salt&pepper noise.

2.2 Experiment A
No signal, Gaussian noise

In the first experiment, we filter pure noise with only a constant value as the ideal, noise-free signal. In such a case the optimal diffusion filtering result – the constant – is reached at time $t = \infty$ with the classical diffusion methods. The experimental results are shown for varied amount of noise and for various filtering methods in Table 1. (The computation was limited to 100 iterations, so $T = 100$ can be understood as 'almost infinity'.)

Fig. 5 shows the obtained filtering quality measured by $\mathrm{MAD}(\mathbf{u}(T) - \widetilde{\mathbf{f}})$ for various filters. The plot gives results for a series of experiments, drawn against the amount of noise in the input image (the horizontal axes represents the standard deviation of noise).

You can see from Table 2 and from Fig. 5 that the noise is in this experiment best removed by the diffusion filters using (piecewise) constant function as their model; these methods include linear diffusion, isotropic and anisotropic NL diffusion. This observation is expected as the noise-free function itself is constant. The monotonicity-enhancing diffusion filter uses a piecewise linear model, which is more general and thus weaker at filtering noise from the constant function. The iterated median filter is easily outperformed by the diffusion filters.

For all filters except the iterated median, the decorrelation criterion yields a good estimate of the optimal stopping time; cf. Table 1.
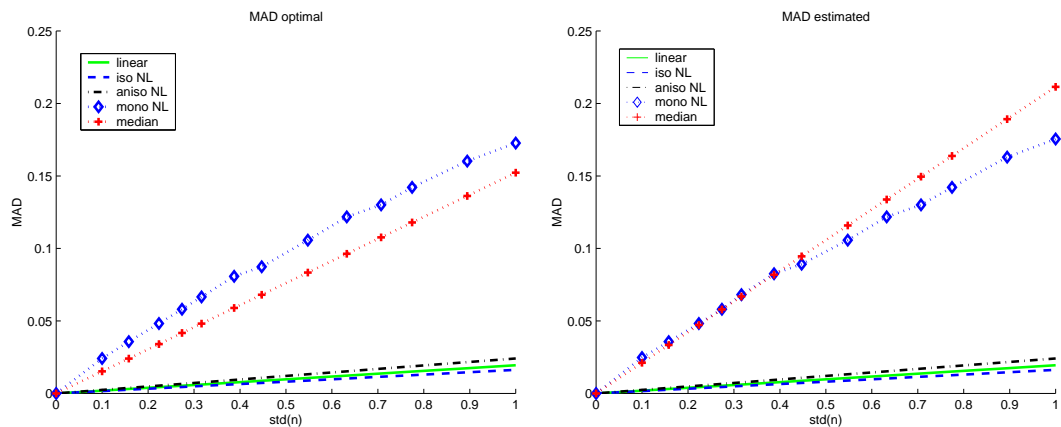
Figure 5: Experiment A. Plots of the error residual $MAD(\mathbf{u}(T) - \widetilde{\mathbf{f}})$ after filtering: optimal for each method and each noise level on the left, with estimated stopping time on the right.

var(n)	linear diff.		iso. NL diff.		aniso. NL diff.		mono. NL diff.		iter. median	
	T_{opt}	T_{corr}	T_{opt}	T_{corr}	T_{opt}	T_{corr}	T_{opt}	T_{corr}	T_{opt}	T_{corr}
0	0	2	0	18	0	6	0	0	0	0
0.01	100	100	100	100	100	100	2	3	45	3
0.025	100	100	100	100	100	100	3	3	45	3
0.05	100	100	100	100	100	100	3	3	45	3
0.075	100	100	100	100	100	100	3	3	45	3
0.1	100	100	100	100	100	100	3	4	45	3
0.15	100	100	100	100	100	100	3	4	45	3
0.2	100	100	100	100	100	100	3	4	45	3
0.3	100	100	100	100	100	100	4	4	45	3
0.4	100	100	100	100	100	100	4	4	45	3
0.5	100	100	100	100	100	100	4	4	45	3
0.6	100	100	100	100	100	100	4	4	45	3
0.8	100	100	100	100	100	100	4	5	45	3
1	100	100	100	100	100	100	4	5	45	3

Table 1: Experiment A: Optimal and estimated values of T.

var(n)	linear diff.		iso. NL diff.		aniso. NL diff.		mono. NL diff.		iter. median	
	D_{opt}	D_{corr}	D_{opt}	D_{corr}	D_{opt}	D_{corr}	D_{opt}	D_{corr}	D_{opt}	D_{corr}
0	0.000	0.000	0.000	0.000	0.000	0.000	0.000	0.000	0.000	0.000
0.01	0.001	0.001	0.001	0.001	0.002	0.002	0.024	0.024	0.015	0.021
0.025	0.003	0.003	0.002	0.002	0.003	0.003	0.035	0.035	0.024	0.033
0.05	0.004	0.004	0.003	0.003	0.005	0.005	0.048	0.048	0.034	0.047
0.075	0.005	0.005	0.004	0.004	0.006	0.006	0.058	0.058	0.041	0.057
0.1	0.006	0.006	0.005	0.005	0.007	0.007	0.066	0.068	0.048	0.066
0.15	0.007	0.007	0.006	0.006	0.009	0.009	0.080	0.082	0.058	0.081
0.2	0.008	0.008	0.007	0.007	0.010	0.010	0.087	0.089	0.068	0.094
0.3	0.010	0.010	0.008	0.008	0.013	0.013	0.105	0.105	0.083	0.115
0.4	0.012	0.012	0.010	0.010	0.015	0.015	0.121	0.121	0.096	0.133
0.5	0.013	0.013	0.011	0.011	0.017	0.017	0.130	0.130	0.107	0.149
0.6	0.015	0.015	0.012	0.012	0.018	0.018	0.142	0.142	0.117	0.163
0.8	0.017	0.017	0.014	0.014	0.021	0.021	0.160	0.162	0.136	0.189
1	0.019	0.019	0.016	0.016	0.024	0.024	0.172	0.175	0.152	0.211

Table 2: Experiment A: Values of $\text{MAD}(\mathbf{u}(T) - \widetilde{\mathbf{f}})$ for optimal and estimated values of the stopping time T.
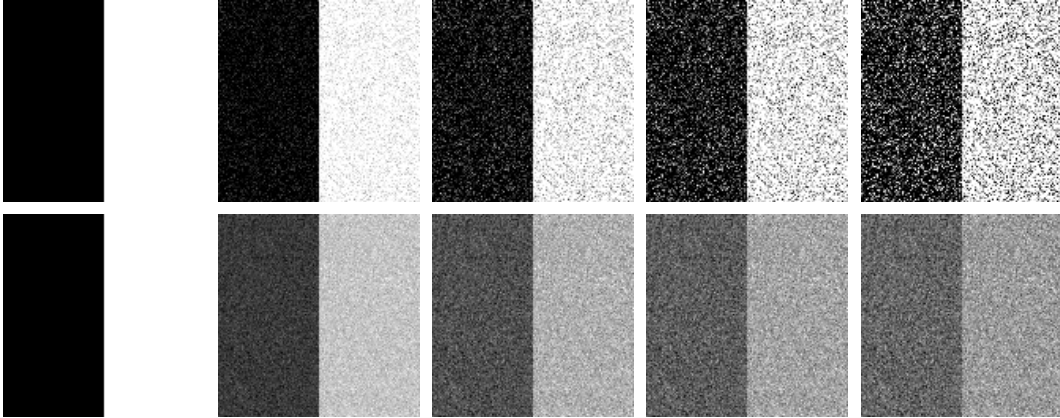
Figure 6: Some of the input images for Experiment B (size 128×128). Increasing amount of noise from left to right from SNR $= \infty$ (no noise) to SNR $= 1$. The top and bottom lines present the same images, at the bottom the grey values are shown rescaled into [0,255].

2.3 Experiment B
Step function in 2D, Gaussian noise

In the second experiment, the ideal signal is a step function in 2D. The noise-free and the noisy images (additive Gaussian noise) are shown in Fig. 6.

What can be seen from the filtering results in Tables 3 and 4 and Figures 7–12:

- The estimation of T yields obsolete results if there is no noise in the input image, especially when isotropic and anisotropic NL diffusion is concerned. However, these errors in the estimation of T lead only to small errors in the distance D_{corr} because other parameters of the diffusion are also estimated from the input images, and the diffusion was kept very slow in the images without noise.

- T seems badly estimated also for other noise levels of the isotropic and anisotropic NL diffusion filters. Still, these methods are best suited for the data properties and even with this bad T outperform all the others in the filtering quality.

- The estimation of T does not work with iterated median filter.

10

var(n)	linear diff.		iso. NL diff.		aniso. NL diff.		mono. NL diff.		iter. median	
	T_{opt}	T_{corr}	T_{opt}	T_{corr}	T_{opt}	T_{corr}	T_{opt}	T_{corr}	T_{opt}	T_{corr}
0	0	2	0	100	0	43	0	1	0	0
162	2	2	100	12	14	7	3	1	45	1
406	3	2	100	18	20	10	4	2	45	1
812	3	3	100	25	28	13	5	3	45	1
1219	4	3	100	28	34	15	5	3	45	1
1625	5	4	100	32	39	16	5	4	45	1
2438	6	4	100	41	46	19	5	4	46	1
3251	7	4	100	45	52	20	6	5	45	1
4877	8	5	100	56	54	21	7	6	45	1
6502	9	6	100	74	47	20	8	7	45	3
8128	10	6	100	72	45	20	9	8	45	3
9754	11	7	100	76	46	21	9	9	45	3
13005	12	8	100	43	51	23	10	11	45	3
16257	14	8	100	32	52	24	11	14	45	3

Table 3: Experiment B: Optimal and estimated values of T.

var(n)	linear diff.		iso. NL diff.		aniso. NL diff.		mono. NL diff.		iter. median	
	D_{opt}	D_{corr}	D_{opt}	D_{corr}	D_{opt}	D_{corr}	D_{opt}	D_{corr}	D_{opt}	D_{corr}
0	0.00	2.34	0.00	0.09	0.00	1.71	0.00	1.02	0.00	0.00
162	4.18	4.18	0.39	0.89	1.65	1.93	3.85	4.69	2.08	4.22
406	5.23	5.27	0.58	1.16	2.16	2.46	4.88	5.44	3.30	6.68
812	6.17	6.17	0.79	1.36	2.56	2.92	5.95	6.25	4.67	9.44
1219	6.78	6.89	0.93	1.54	2.81	3.23	6.73	7.25	5.72	11.57
1625	7.27	7.29	1.04	1.65	3.02	3.53	7.46	7.59	6.60	13.36
2438	8.00	8.15	1.15	1.76	3.34	3.92	8.70	8.90	8.09	16.36
3251	8.57	8.87	1.18	1.84	3.60	4.31	9.57	9.66	9.34	18.89
4877	9.41	9.72	1.28	1.83	4.07	4.96	10.86	10.94	11.44	23.14
6502	10.07	10.33	1.38	1.66	4.59	5.65	11.82	11.87	13.20	17.80
8128	10.60	11.05	1.52	1.84	5.03	6.18	12.62	12.64	14.75	19.89
9754	11.07	11.41	1.66	1.93	5.37	6.51	13.31	13.31	16.15	21.78
13005	11.84	12.21	1.88	3.08	5.89	7.07	14.48	14.48	18.58	25.08
16257	12.48	13.06	2.49	4.19	6.41	7.70	15.45	15.64	20.69	27.96

Table 4: Experiment B: Values of $\mathrm{MAD}(\mathbf{u}(T) - \widetilde{\mathbf{f}})$ for optimal and estimated values of stopping time T.
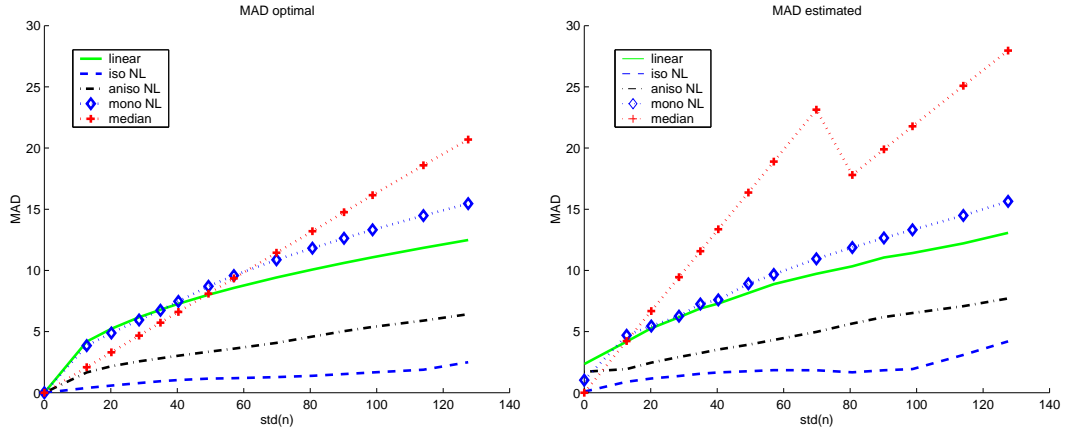
Figure 7: Experiment B. Plots of the error residual $MAD(\mathbf{u}(T) - \widetilde{\mathbf{f}})$ after filtering: optimal for each method and each noise level on the left, with estimated stopping time on the right.
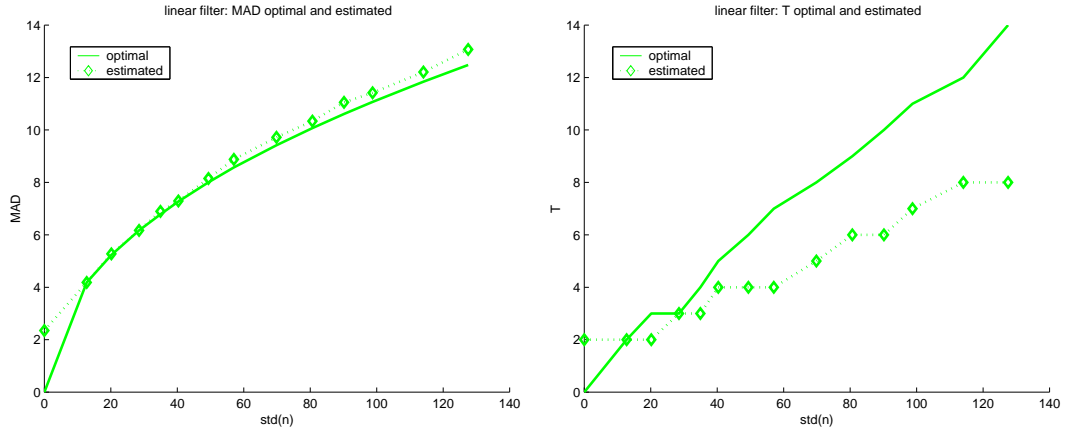
Figure 8: Experiment B, linear diffusion. Values of $MAD(\mathbf{u}(T) - \widetilde{\mathbf{f}})$ for the optimal and estimated time on the left; the optimal and estimated values of time T on the right.
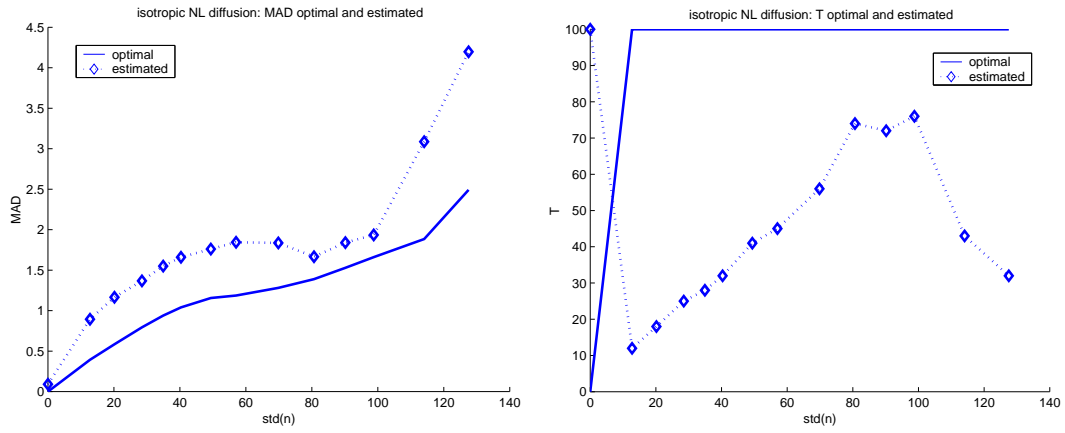
Figure 9: Experiment B, isotropic NL diffusion. Values of $MAD(\mathbf{u}(T) - \widetilde{\mathbf{f}})$ for the optimal and estimated time on the left; the optimal and estimated values of time T on the right.
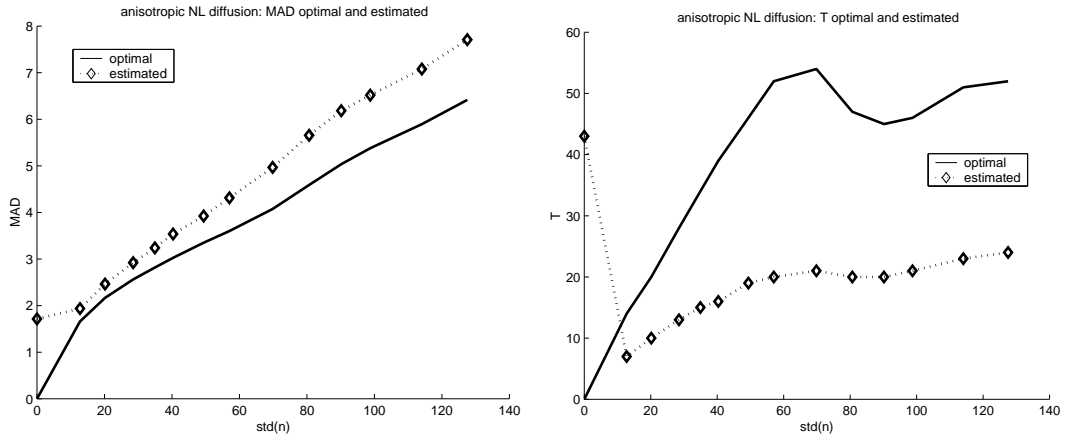
Figure 10: Experiment B, anisotropic NL diffusion. Values of $\mathrm{MAD}(\mathbf{u}(T) - \widetilde{\mathbf{f}})$ for the optimal and estimated time on the left; the optimal and estimated values of time T on the right.
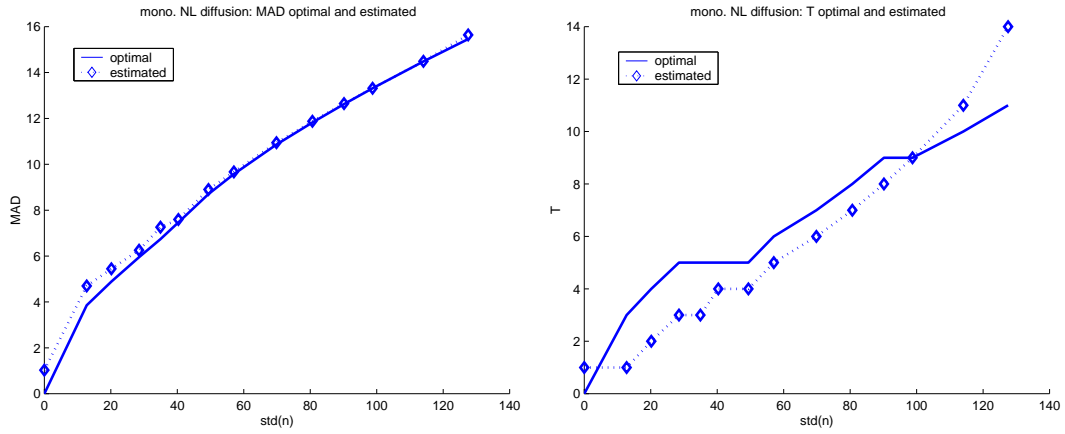
Figure 11: Experiment B, monotonicity-enhancing NL diffusion. Values of $\mathrm{MAD}(\mathbf{u}(T) - \widetilde{\mathbf{f}})$ for the optimal and estimated time on the left; the optimal and estimated values of time T on the right.
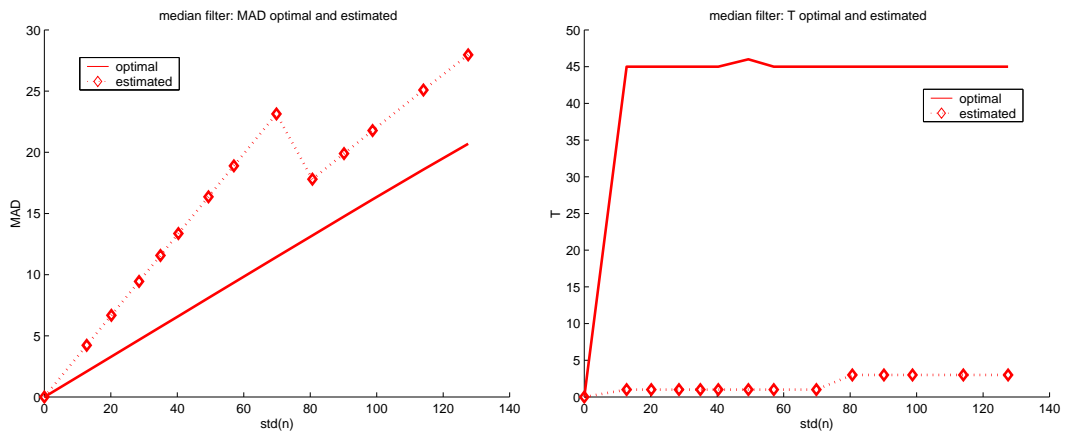
Figure 12: Experiment B, iterated median filter. Values of $\mathrm{MAD}(\mathbf{u}(T) - \widetilde{\mathbf{f}})$ for the optimal and estimated time on the left; the optimal and estimated values of time T on the right.

13
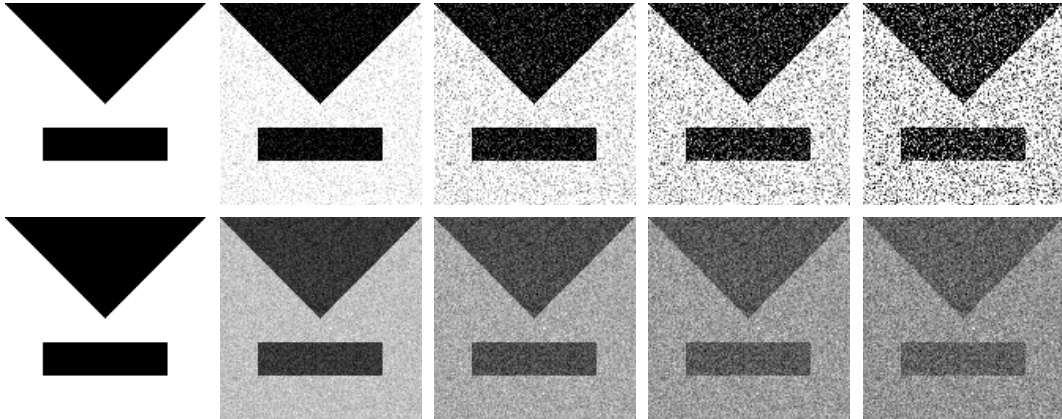
Figure 13: Some of the input images for Experiment C (size 128×128). Increasing amount of noise from left to right from SNR $= \infty$ (no noise) to SNR $= 1$. The top and bottom lines present the same images, at the bottom the grey values are shown rescaled into [0,255].

2.4 Experiment C
Triangle and rectangle, Gaussian noise

The ideal and noisy signals used in Experiment C are shown in Fig. 13. We present the filtering results in Tables 5 and 6, and Figures 14–19. Some observations:

- As in Experiment B, the estimation of T yields obsolete results if there is no noise in the input image. Again, these errors have only moderate effect on the filtering quality.

- The optimal and estimated stopping times are in a very good correspondence with linear diffusion filter. Also the anisotropic diffusion reveals relatively good estimation results.

- Again, there is a relatively high error in the estimation of T for isotropic NL diffusion. Again however, the filtering performance of this filter is the best of all in spite of these errors.

- The estimation of T does not work at all with monotonicity-ehnancing diffusion or the iterated median filter.

var(n)	linear diff.		iso. NL diff.		aniso. NL diff.		mono. NL diff.		iter. median	
	T_{opt}	T_{corr}	T_{opt}	T_{corr}	T_{opt}	T_{corr}	T_{opt}	T_{corr}	T_{opt}	T_{corr}
0	0	2	0	100	0	39	0	43	0	1
148	1	2	88	8	8	4	1	38	45	1
370	1	2	100	11	10	6	2	36	45	1
740	2	2	100	16	13	9	3	33	45	1
1111	2	2	100	17	15	10	3	32	45	1
1481	2	3	100	20	17	11	3	31	45	1
2222	2	3	100	24	20	13	3	29	45	1
2963	3	3	100	28	22	14	3	28	45	1
4445	3	3	100	37	24	15	4	27	46	1
5927	3	4	100	43	25	15	4	26	45	1
7409	4	4	100	45	25	15	4	25	45	1
8891	4	4	100	53	24	16	5	25	45	1
11854	4	5	100	38	22	16	5	24	45	3
14818	5	5	45	20	19	16	6	24	45	3

Table 5: Experiment C: Optimal and estimated values of T.

var(n)	linear diff.		iso. NL diff.		aniso. NL diff.		mono. NL diff.		iter. median	
	D_{opt}	D_{corr}	D_{opt}	D_{corr}	D_{opt}	D_{corr}	D_{opt}	D_{corr}	D_{opt}	D_{corr}
0	0.00	7.14	0.00	0.31	0.00	4.83	0.00	31.46	0.00	0.07
148	7.18	8.59	0.82	1.41	2.68	3.21	5.89	30.96	2.33	4.21
370	8.79	9.49	1.18	1.95	3.43	3.82	7.40	30.87	3.64	6.62
740	10.53	10.53	1.56	2.40	4.17	4.38	8.80	30.78	5.11	9.33
1111	11.34	11.34	1.70	2.73	4.59	4.83	9.74	30.67	6.25	11.42
1481	12.02	12.58	1.87	2.93	4.96	5.25	10.58	30.59	7.20	13.17
2222	13.19	13.44	2.07	3.20	5.49	5.77	12.02	30.10	8.80	16.11
2963	14.16	14.16	2.12	3.30	5.87	6.20	13.25	30.00	10.15	18.60
4445	15.40	15.40	2.22	3.30	6.45	6.92	15.10	30.01	12.42	22.76
5927	16.45	16.56	2.23	3.26	6.93	7.60	16.51	29.94	14.30	26.25
7409	17.33	17.33	2.26	3.34	7.45	8.27	17.68	29.80	15.95	29.31
8891	18.02	18.02	2.34	3.21	8.10	8.73	18.60	30.11	17.40	32.05
11854	19.26	19.27	2.67	4.13	9.63	10.09	20.13	30.09	19.93	25.49
14818	20.22	20.22	5.15	6.49	11.24	11.48	21.35	30.54	22.05	28.31

Table 6: Experiment C: Values of $\mathrm{MAD}(\mathbf{u}(T) - \widetilde{\mathbf{f}})$ for optimal and estimated values of stopping time T.
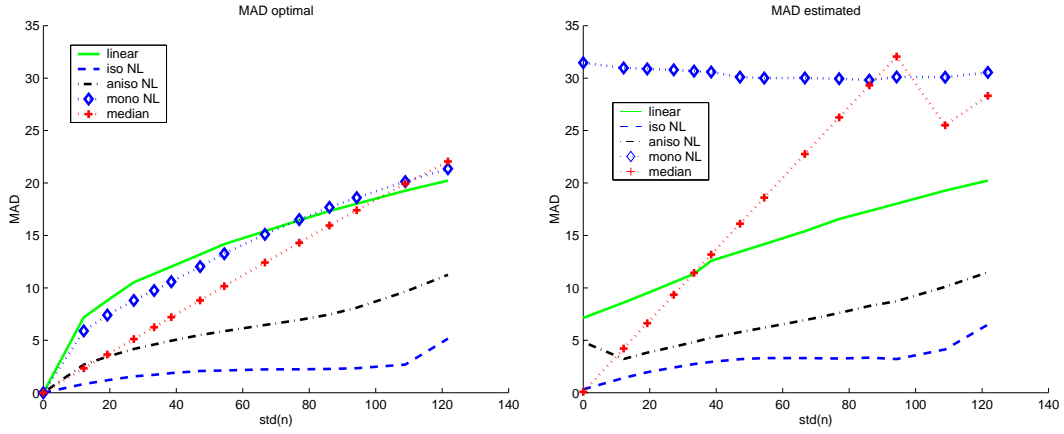
Figure 14: Experiment C. Plots of the error residual $MAD(\mathbf{u}(T) - \widetilde{\mathbf{f}})$ after filtering: optimal for each method and each noise level on the left, with estimated stopping time on the right.
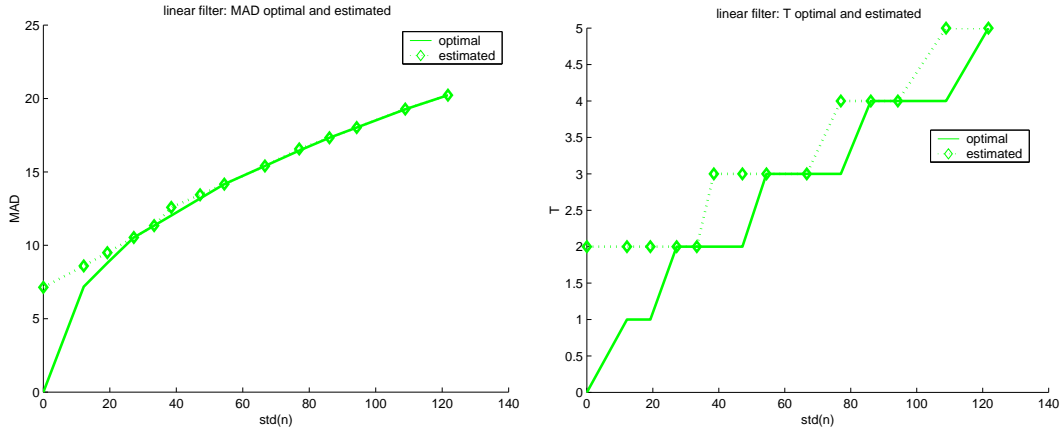
Figure 15: Experiment C, linear diffusion. Values of $\mathrm{MAD}(\mathbf{u}(T) - \widetilde{\mathbf{f}})$ for the optimal and estimated time on the left; the optimal and estimated values of time T on the right.
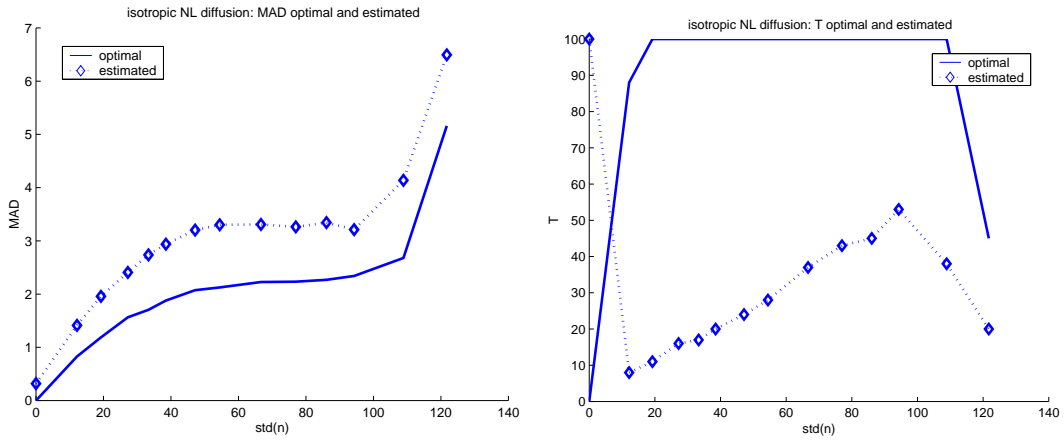
Figure 16: Experiment C, isotropic NL diffusion. Values of $\mathrm{MAD}(\mathbf{u}(T) - \widetilde{\mathbf{f}})$ for the optimal and estimated time on the left; the optimal and estimated values of time T on the right.

16
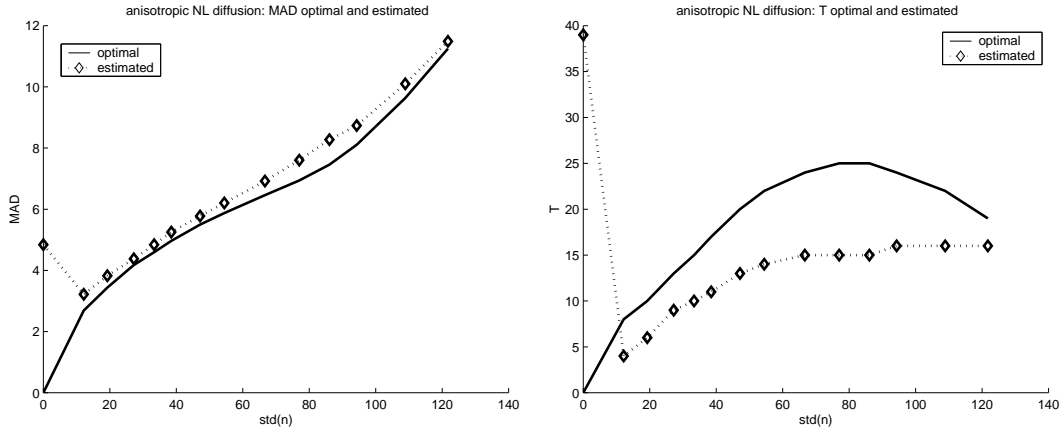
Figure 17: Experiment C, anisotropic NL diffusion. Values of $\mathrm{MAD}(\mathbf{u}(T)-\widetilde{\mathbf{f}})$ for the optimal and estimated time on the left; the optimal and estimated values of time T on the right.
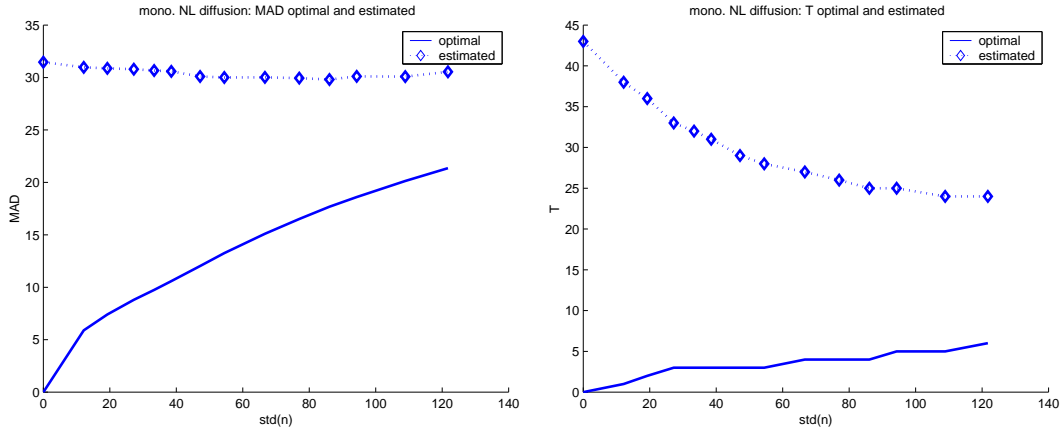
Figure 18: Experiment C, monotonicity-enhancing NL diffusion. Values of $\mathrm{MAD}(\mathbf{u}(T) - \widetilde{\mathbf{f}})$ for the optimal and estimated time on the left; the optimal and estimated values of time T on the right.
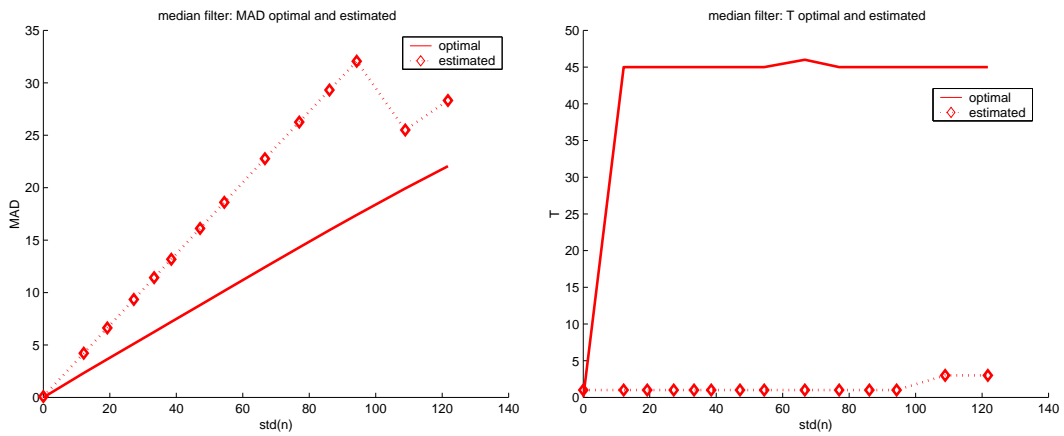
Figure 19: Experiment C, iterated median filter. Values of $\mathrm{MAD}(\mathbf{u}(T) - \widetilde{\mathbf{f}})$ for the optimal and estimated time on the left; the optimal and estimated values of time T on the right.
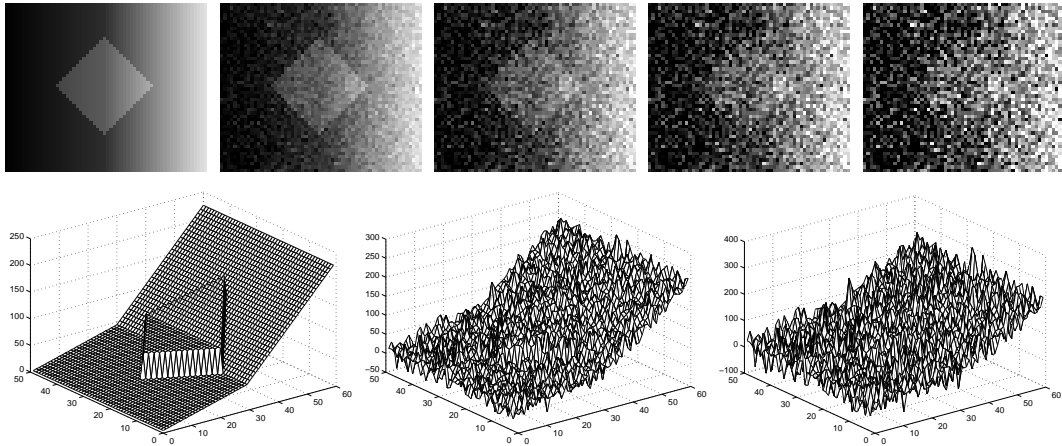
Figure 20: Some of the input images for Experiment D (size 60×50). Top: increasing amount of noise from left to right from SNR $= \infty$ (no noise) to SNR $= 1$. Bottom: 3D mesh of three least noisy images from the top line (SNR $= \infty$, 20 and 5, respectively).

2.5 Experiment D
Inclined surface, Gaussian noise

In Experiment D, we use piecewise linear and piecewise increasing surface as the ideal data (see Fig. 20). Such data properties are not covered well by the classical diffusion filters (linear, isotropic or anisotropic nonlinear) which use (piecewise) constant as their model. On the other hand, this kind of data is exactly suitable for the monotonicity-enhancing NL diffusion filter. Let us observe Tables 7–8 and Figures 21–26 and see whether the results reflect these expectations.

- We obtain very good estimates of T for the linear, isotropic and anisotropic NL diffusion (except the no-noise input image with isotropic NL diffusion filter).

- Monotonicity-enhancing NL diffusion filter gets very good estimates of T for smaller amounts of noise (up to SNR $= 5$), for more noise the estimates deviate more from the optimum. Also the filtering performance confirms expectations and this filter which is based on a piecewise-linear model gives the best results, measured both visually (cf. Figure 69 on page 56) and in the MAD distance from ideal data. The numerical difference from the anisotropic NL diffusion filter is not significant, though.

- Here as before, the estimation of T does not work with iterated median filtering.

	linear diff.		iso. NL diff.		aniso. NL diff.		mono. NL diff.		iter. median	
$\mathrm{var}(n)$	T_{opt}	T_{corr}	T_{opt}	T_{corr}	T_{opt}	T_{corr}	T_{opt}	T_{corr}	T_{opt}	T_{corr}
0	0	1	0	100	0	2	0	1	0	1
46	2	1	3	2	6	5	3	2	2	1
116	2	2	4	3	8	7	3	2	5	1
233	3	2	5	3	10	8	4	3	13	1
350	3	3	6	4	11	9	4	4	21	1
467	4	3	6	4	12	9	5	5	21	1
700	4	3	9	5	13	10	5	6	21	1
934	5	4	9	5	13	11	6	7	21	1
1401	6	4	8	6	13	12	6	10	22	1
1868	6	5	9	7	14	13	7	13	24	1
2336	7	5	9	7	15	14	7	16	24	3
2803	7	5	9	7	15	15	8	23	24	3
3737	8	6	9	8	17	16	9	28	26	3
4672	9	7	10	9	18	17	9	32	26	3

Table 7: Experiment D: Optimal and estimated values of T

	linear diff.		iso. NL diff.		aniso. NL diff.		mono. NL diff.		iter. median	
$\mathrm{var}(n)$	D_{opt}	D_{corr}	D_{opt}	D_{corr}	D_{opt}	D_{corr}	D_{opt}	D_{corr}	D_{opt}	D_{corr}
0	0.00	1.17	0.00	8.22	0.00	0.32	0.00	0.62	0.00	0.16
46	2.52	2.60	2.35	2.50	2.37	2.41	2.08	2.10	2.33	2.57
116	3.04	3.04	3.12	3.25	3.03	3.04	2.79	2.95	3.10	3.80
233	3.57	3.67	3.74	4.15	3.55	3.59	3.53	3.57	3.96	5.21
350	3.92	3.92	4.12	4.35	3.84	3.89	4.01	4.01	4.55	6.31
467	4.20	4.24	4.38	4.76	4.05	4.16	4.40	4.40	5.05	7.23
700	4.64	4.78	4.62	5.03	4.41	4.53	4.99	5.01	5.80	8.76
934	4.99	5.02	4.91	5.48	4.78	4.84	5.48	5.53	6.42	10.04
1401	5.54	5.68	5.56	5.86	5.42	5.44	6.27	6.56	7.45	12.19
1868	5.97	6.04	6.01	6.12	5.89	5.91	6.92	7.52	8.32	14.00
2336	6.34	6.48	6.33	6.52	6.28	6.29	7.48	8.39	9.09	10.78
2803	6.66	6.89	6.62	6.87	6.62	6.62	7.98	9.64	9.77	11.72
3737	7.21	7.38	7.18	7.27	7.17	7.17	8.84	10.95	10.98	13.40
4672	7.67	7.79	7.62	7.65	7.62	7.63	9.58	12.05	12.08	14.91

Table 8: Experiment D: Values of $\mathrm{MAD}(\mathbf{u}(T) - \widetilde{\mathbf{f}})$ for optimal and estimated values of stopping time T.
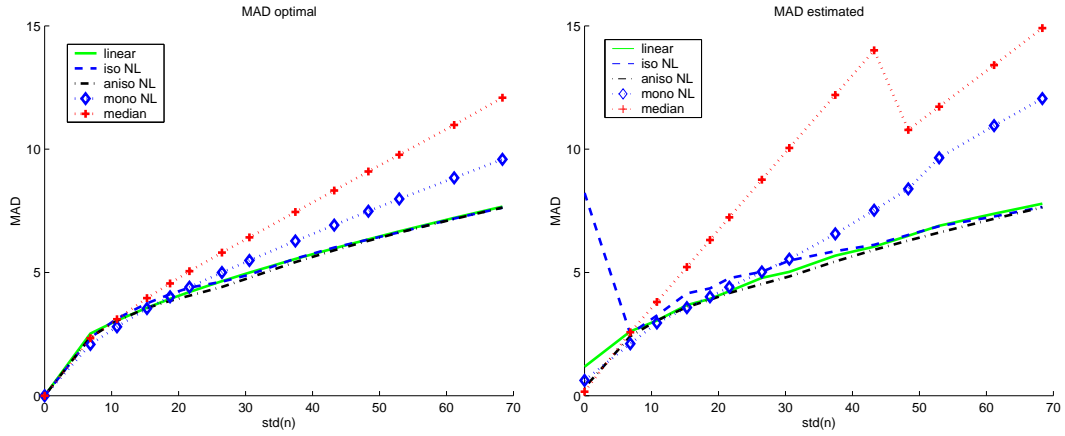
Figure 21: Experiment D. Plots of the error residual $MAD(\mathbf{u}(T) - \widetilde{\mathbf{f}})$ after filtering: optimal for each method and each noise level on the left, with estimated stopping time on the right.
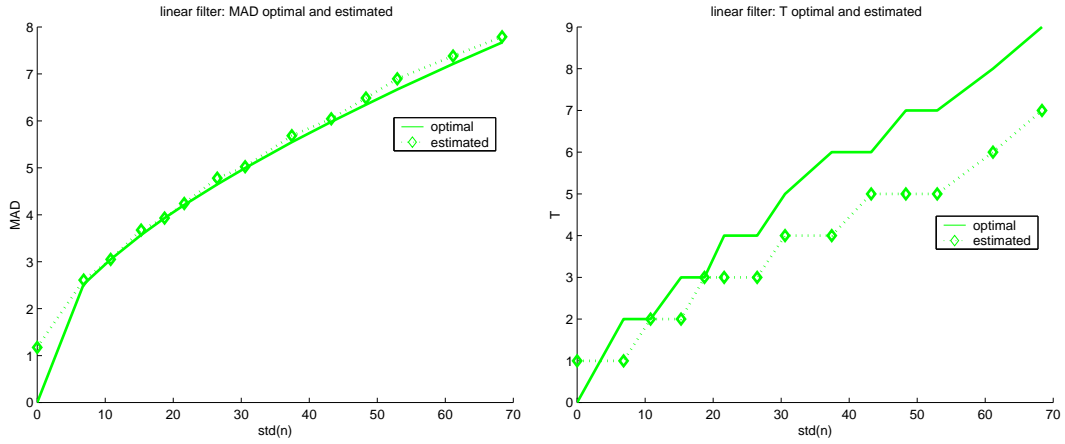
Figure 22: Experiment D, linear diffusion. Values of $\mathrm{MAD}(\mathbf{u}(T) - \widetilde{\mathbf{f}})$ for the optimal and estimated time on the left; the optimal and estimated values of time T on the right.
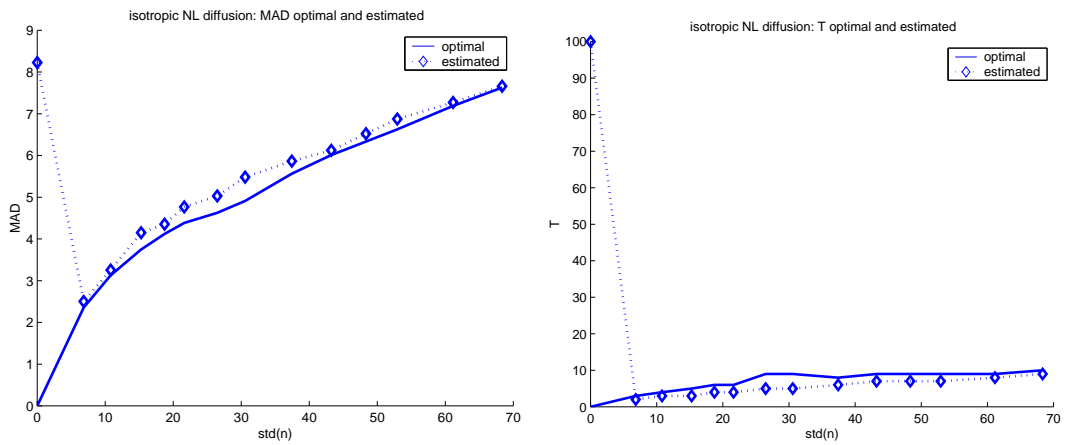
Figure 23: Experiment D, isotropic NL diffusion. Values of $\mathrm{MAD}(\mathbf{u}(T) - \widetilde{\mathbf{f}})$ for the optimal and estimated time on the left; the optimal and estimated values of time T on the right.
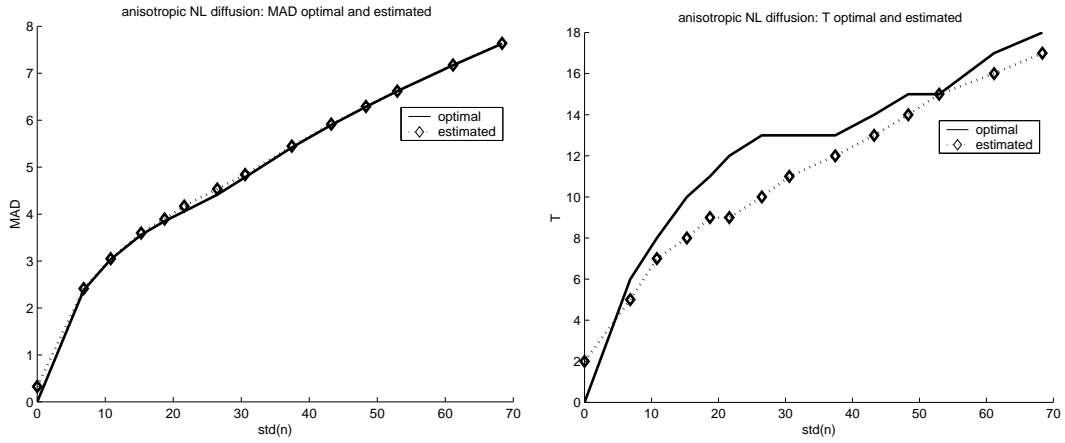
Figure 24: Experiment D, anisotropic NL diffusion. Values of $\mathrm{MAD}(\mathbf{u}(T)-\widetilde{\mathbf{f}})$ for the optimal and estimated time on the left; the optimal and estimated values of time T on the right.
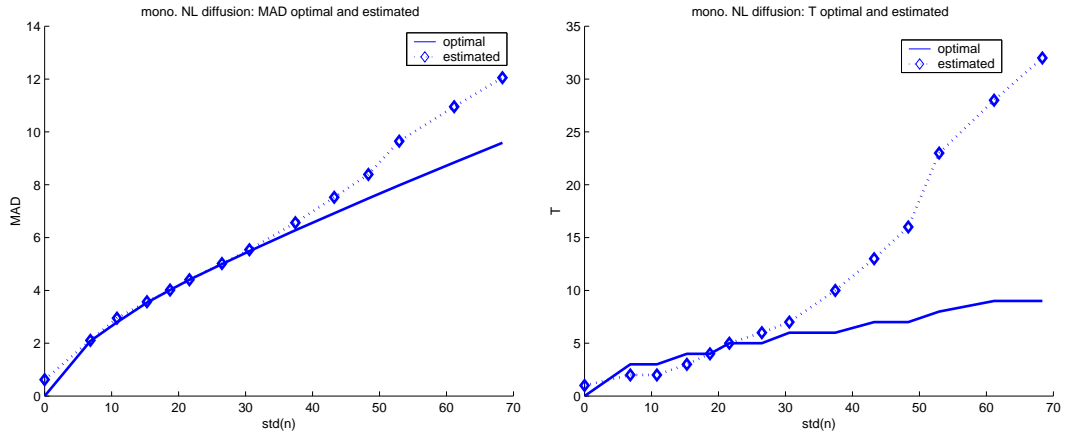
Figure 25: Experiment D, monotonicity-enhancing NL diffusion. Values of $\mathrm{MAD}(\mathbf{u}(T)-\widetilde{\mathbf{f}})$ for the optimal and estimated time on the left; the optimal and estimated values of time T on the right.
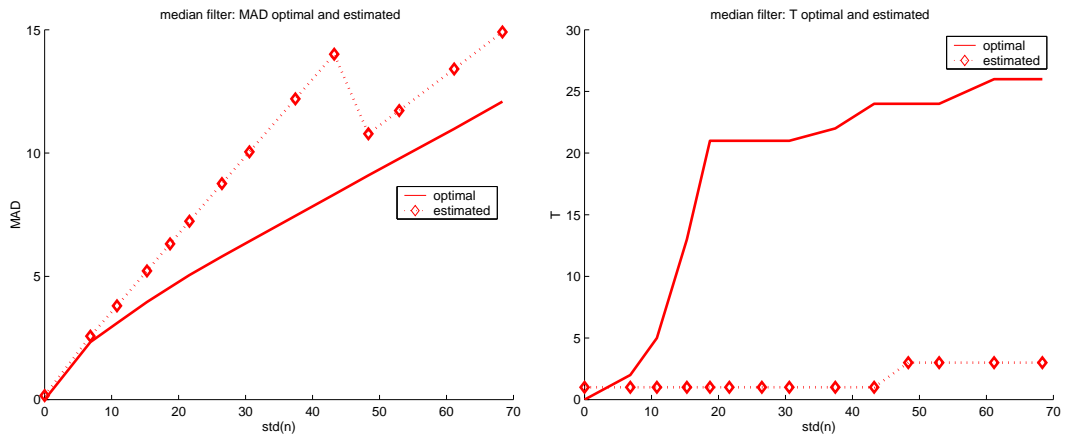
Figure 26: Experiment D, iterated median filter. Values of $\mathrm{MAD}(\mathbf{u}(T)-\widetilde{\mathbf{f}})$ for the optimal and estimated time on the left; the optimal and estimated values of time T on the right.
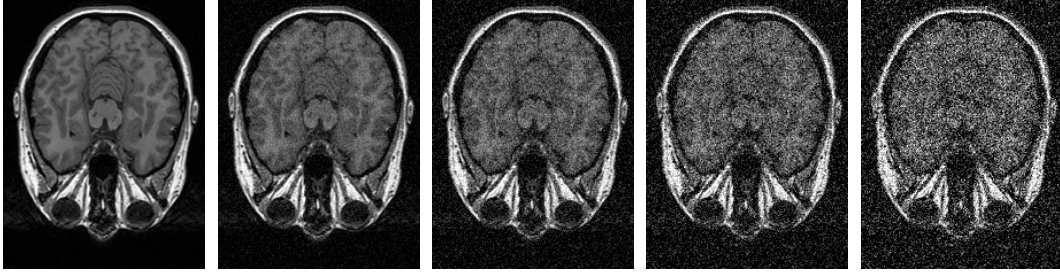
Figure 27: Some of the input images for Experiment E (size 176×236). Increasing amount of artificially added noise from left to right from SNR $= \infty$ (no noise) to SNR $= 1$.
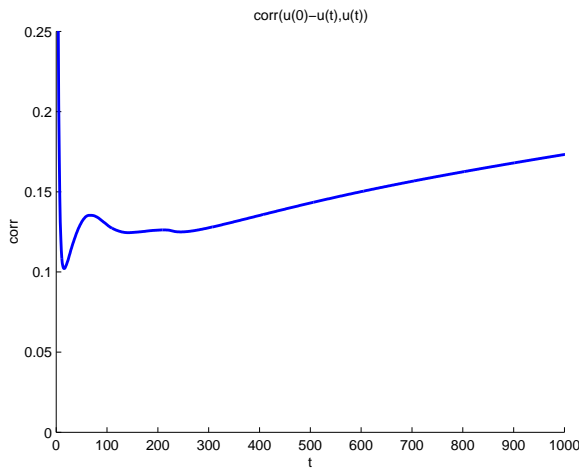
Figure 28: Example of irregular behaviour of $\mathrm{corr}(\mathbf{u}(0) - \mathbf{u}(t), \mathbf{u}(t))$. Experiment E (MRI data), additive Gaussian noise of SNR $= 2$, anisotropic NL diffusion filter. The optimal T_{opt} was equal to 8, this graph attains its minimum at $t = 15$.

2.6 Experiment E
MRI image, Gaussian noise

In Experiment E we use a slice of MRI data as the ideal signal, see Fig. 27. The good aspect in this experiment is that the data are more realistic than the artificial examples before. On the other hand, there will be some amount of noise present already in the original image which we declare to be noise-free; this noise will bias the performance of the time estimation procedures, and the 'optimal' stopping time minimizing the MAD distance to input data does not necessarily correspond to the smallest noise artefacts in the filtered signal.

In this experiment, we observed for the first time that the graph of $\mathrm{corr}\big(\mathbf{u}(0) - \mathbf{u}(t), \mathbf{u}(t)\big)$ is not always unimodal. The case is shown in Fig. 28. Other experimental results are presented in Tables 9–10 and Figures 29–34. Let us comment on them briefly.

- Here as before, the estimation of T does not work with iterated median filtering.

- Quite surprisingly, the estimation of T gives completely obsolete results for linear diffusion and for monotonicity-enhancing NL diffusion.

- The estimation works well for isotropic and anisotropic NL diffusion filters. Relatively worse estimation results for smaller amount of artificialy added noise are influenced by the noise present already in the original input data as discussed above.

var(n)	linear diff.		iso. NL diff.		aniso. NL diff.		mono. NL diff.		iter. median	
	T_{opt}	T_{corr}	T_{opt}	T_{corr}	T_{opt}	T_{corr}	T_{opt}	T_{corr}	T_{opt}	T_{corr}
0	0	100	0	48	0	23	0	74	0	1
31	0	100	1	32	2	7	0	71	0	1
79	0	100	2	37	3	7	1	69	1	1
158	1	100	2	28	4	9	1	66	1	1
238	1	100	3	27	4	10	1	65	1	1
317	1	100	3	16	5	10	1	63	2	1
476	1	100	3	12	6	11	1	62	2	1
635	1	100	4	12	6	12	1	60	3	1
953	1	100	4	11	7	13	2	56	4	1
1271	2	99	4	12	7	14	2	53	6	1
1589	2	97	5	12	8	15	2	50	6	1
1907	2	96	5	12	8	15	2	48	7	1
2543	2	94	5	12	8	15	3	43	8	1
3179	2	93	6	11	9	16	3	40	9	1

Table 9: Optimal and estimated values of T for varied amount of noise and for various filtering methods in Experiment E.

var(n)	linear diff.		iso. NL diff.		aniso. NL diff.		mono. NL diff.		iter. median	
	D_{opt}	D_{corr}	D_{opt}	D_{corr}	D_{opt}	D_{corr}	D_{opt}	D_{corr}	D_{opt}	D_{corr}
0	0.00	27.81	0.00	7.86	0.00	9.09	0.00	27.10	0.00	3.88
31	4.49	27.82	3.36	7.64	3.45	5.24	4.49	27.04	4.49	5.23
79	7.11	27.83	4.65	8.77	4.60	5.75	5.78	27.00	6.11	6.11
158	7.96	27.84	5.70	9.15	5.60	6.85	6.51	26.84	7.15	7.15
238	8.44	27.85	6.47	9.71	6.26	7.50	7.14	26.86	7.97	7.97
317	8.86	27.86	6.99	9.32	6.76	7.83	7.70	26.76	8.49	8.67
476	9.61	27.87	7.81	9.42	7.50	8.53	8.69	26.85	9.35	9.85
635	10.27	27.88	8.45	9.96	8.06	9.17	9.56	26.80	10.06	10.83
953	11.43	27.90	9.41	10.70	8.98	10.13	10.54	26.70	11.09	12.52
1271	12.28	27.88	10.16	11.70	9.71	11.01	11.31	26.66	11.85	13.98
1589	12.72	27.83	10.73	12.16	10.28	11.65	12.00	26.57	12.51	15.27
1907	13.14	27.81	11.22	12.56	10.76	12.02	12.64	26.59	13.08	16.44
2543	13.91	27.77	12.03	13.44	11.67	12.84	13.64	26.42	14.11	18.55
3179	14.61	27.76	12.67	13.78	12.38	13.68	14.39	26.41	15.03	20.41

Table 10: Optimal and estimated values of $\mathrm{MAD}(\mathbf{u}(T) - \widetilde{\mathbf{f}})$ for varied amount of noise and for various filtering methods in Experiment E.
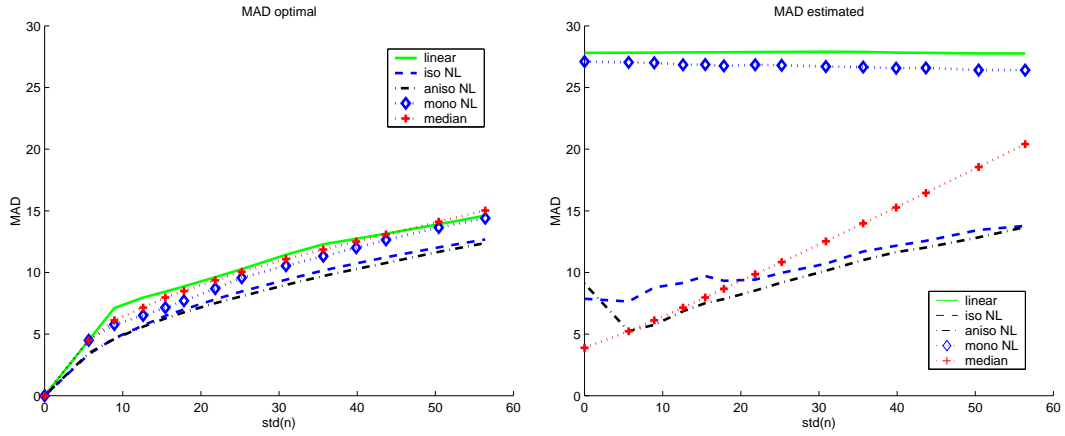
Figure 29: Experiment E. Plots of the error residual $MAD(\mathbf{u}(T) - \widetilde{\mathbf{f}})$ after filtering: optimal for each method and each noise level on the left, with estimated stopping time on the right.
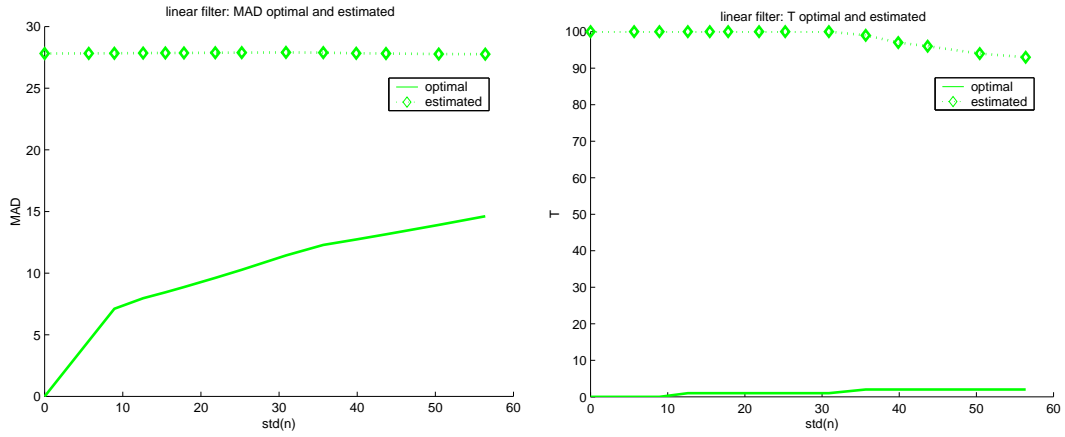
Figure 30: Experiment E, linear diffusion. Values of $\mathrm{MAD}(\mathbf{u}(T) - \widetilde{\mathbf{f}})$ for the optimal and estimated time on the left; the optimal and estimated values of time T on the right.
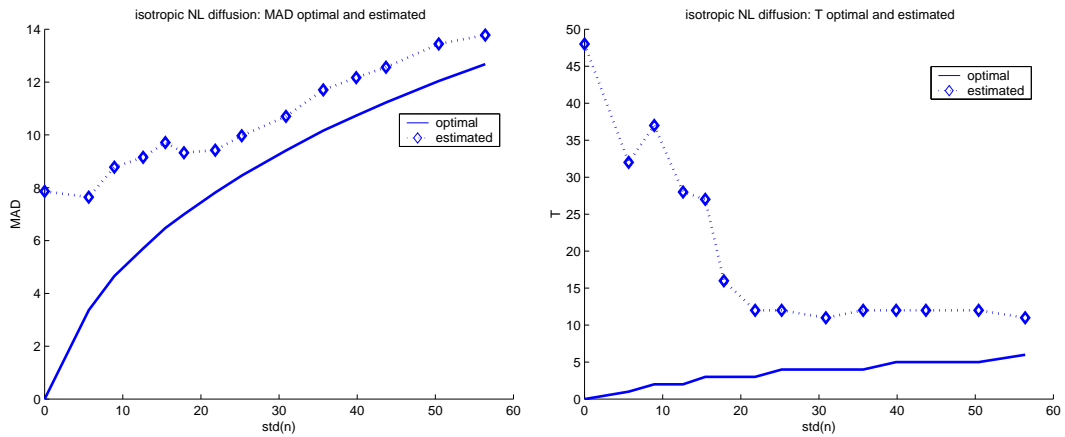
Figure 31: Experiment E, isotropic NL diffusion. Values of $\mathrm{MAD}(\mathbf{u}(T) - \widetilde{\mathbf{f}})$ for the optimal and estimated time on the left; the optimal and estimated values of time T on the right.
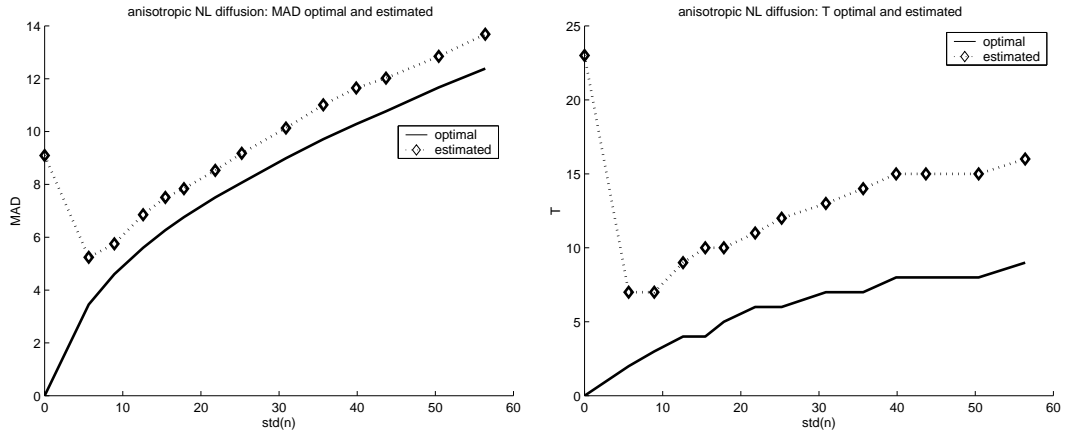
Figure 32: Experiment E, anisotropic NL diffusion. Values of $\text{MAD}(\mathbf{u}(T) - \widetilde{\mathbf{f}})$ for the optimal and estimated time on the left; the optimal and estimated values of time T on the right.
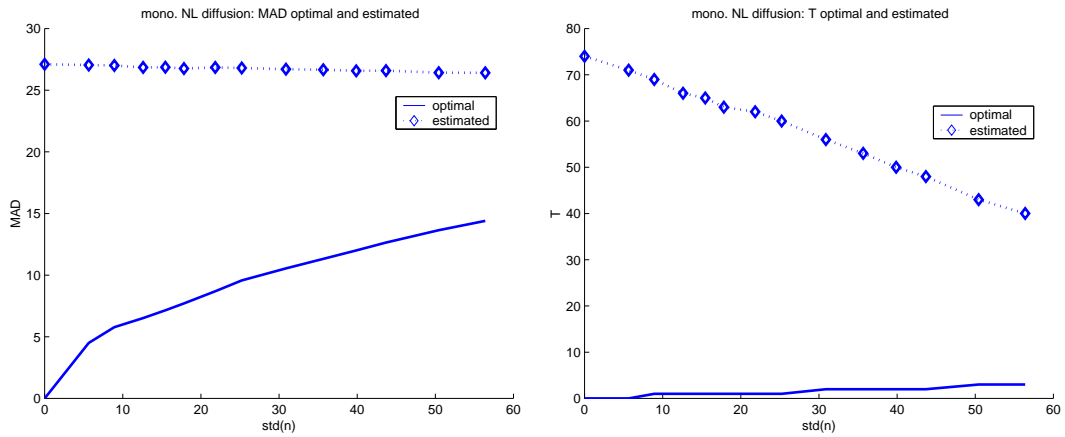
Figure 33: Experiment E, monotonicity-enhancing NL diffusion. Values of $\text{MAD}(\mathbf{u}(T) - \widetilde{\mathbf{f}})$ for the optimal and estimated time on the left; the optimal and estimated values of time T on the right.
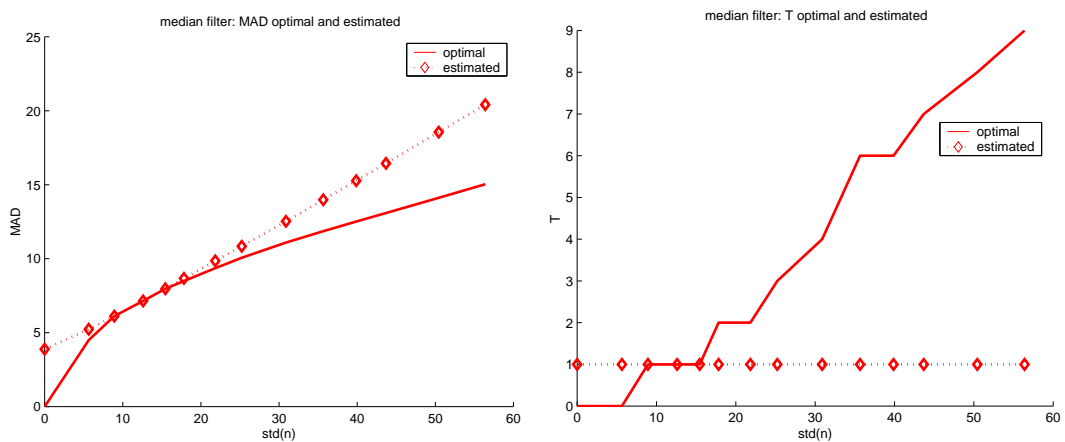
Figure 34: Experiment E, iterated median filter. Values of $\text{MAD}(\mathbf{u}(T) - \widetilde{\mathbf{f}})$ for the optimal and estimated time on the left; the optimal and estimated values of time T on the right.

Figure 35: Some of the input images for Experiment F (size 433×437). Increasing amount of noise from left to right from SNR $= \infty$ (no noise) to SNR $= 1$.

2.7 Experiment F
Cymbidium data, Gaussian noise

Some of the input images for experiment F are seen in Fig. 35. Unlike the MRI image of previous section, the original image here does not contain much noise. What results were obtained in this case (see Tables 11–12 and Figures 36–41):

- The estimation of T does not work with iterated median filtering and with monotonicity-enhancing NL diffusion.

- The stopping time estimated for linear and nonlinear diffusion (isotropic and anisotropic) corresponds very well to the optimal values.

- The isotropic and anisotropic NL diffusion yields the best filtering performance, both for the optimal and estimated stopping time T.

var(n)	linear diff. T_{opt}	linear diff. T_{corr}	iso. NL diff. T_{opt}	iso. NL diff. T_{corr}	aniso. NL diff. T_{opt}	aniso. NL diff. T_{corr}	mono. NL diff. T_{opt}	mono. NL diff. T_{corr}	iter. median T_{opt}	iter. median T_{corr}
0	0	3	0	3	0	2	0	61	0	1
44	1	3	2	4	4	6	1	64	2	62
110	1	3	4	6	6	8	2	65	4	5
221	2	3	5	7	8	11	2	66	10	1
332	2	3	5	8	8	11	3	67	17	1
443	2	3	6	9	9	13	3	67	34	1
665	2	4	6	10	10	14	3	67	43	1
887	3	4	7	10	11	15	4	66	45	1
1330	3	5	7	10	12	16	4	64	39	1
1774	4	5	8	11	13	17	5	62	45	3
2218	4	6	8	12	13	17	5	60	47	3
2661	5	6	9	12	14	18	6	58	51	3
3549	6	7	9	12	14	18	6	53	43	3
4436	6	7	9	12	15	19	7	48	51	3

Table 11: Optimal and estimated values of T for varied amount of noise and for various filtering methods in Experiment F.

var(n)	linear diff. D_{opt}	linear diff. D_{corr}	iso. NL diff. D_{opt}	iso. NL diff. D_{corr}	aniso. NL diff. D_{opt}	aniso. NL diff. D_{corr}	mono. NL diff. D_{opt}	mono. NL diff. D_{corr}	iter. median D_{opt}	iter. median D_{corr}
0	0.00	4.95	0.00	1.56	0.00	1.04	0.00	19.51	0.00	1.90
44	3.57	5.09	2.61	2.73	2.58	2.67	3.14	19.16	3.36	3.62
110	4.33	5.27	3.26	3.43	3.16	3.25	4.00	19.03	4.08	4.08
221	5.11	5.54	3.83	3.96	3.68	3.84	4.66	19.06	4.72	5.88
332	5.48	5.78	4.20	4.42	4.05	4.18	5.16	19.17	5.20	6.90
443	5.81	6.00	4.50	4.69	4.32	4.49	5.52	19.18	5.61	7.77
665	6.38	6.64	4.94	5.19	4.77	4.96	6.12	19.23	6.29	9.24
887	6.73	6.90	5.29	5.52	5.14	5.36	6.60	19.16	6.87	10.50
1330	7.34	7.54	5.83	5.98	5.73	5.92	7.32	19.07	7.86	12.61
1774	7.78	7.87	6.26	6.44	6.19	6.38	7.88	19.00	8.69	10.31
2218	8.16	8.30	6.62	6.85	6.59	6.72	8.33	18.91	9.42	11.32
2661	8.47	8.55	6.93	7.14	6.94	7.10	8.71	18.81	10.08	12.23
3549	9.00	9.08	7.47	7.64	7.58	7.71	9.36	18.46	11.26	13.86
4436	9.42	9.44	7.96	8.10	8.13	8.30	9.88	18.01	12.30	15.30

Table 12: Optimal and estimated values of $\text{MAD}(\mathbf{u}(T) - \widetilde{\mathbf{f}})$ for varied amount of noise and for various filtering methods in Experiment F.
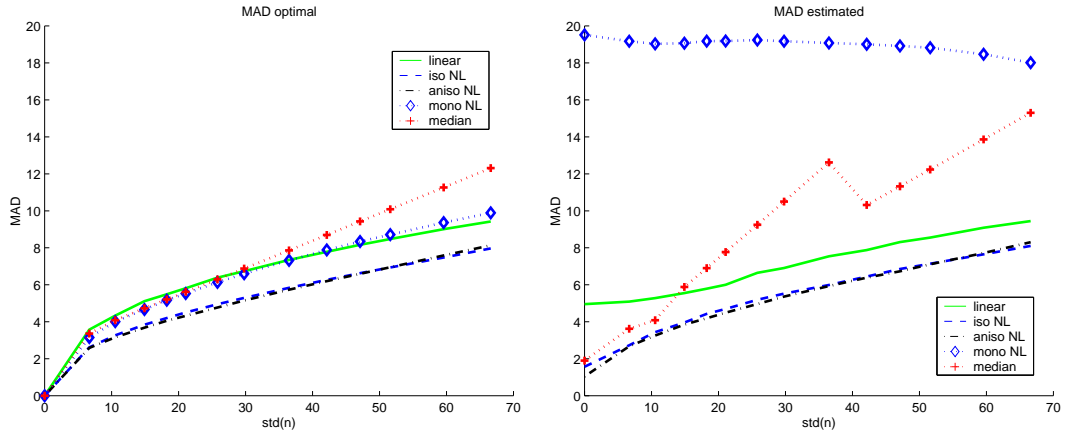
Figure 36: Experiment F. Plots of the error residual $MAD(\mathbf{u}(T) - \widetilde{\mathbf{f}})$ after filtering: optimal for each method and each noise level on the left, with estimated stopping time on the right.
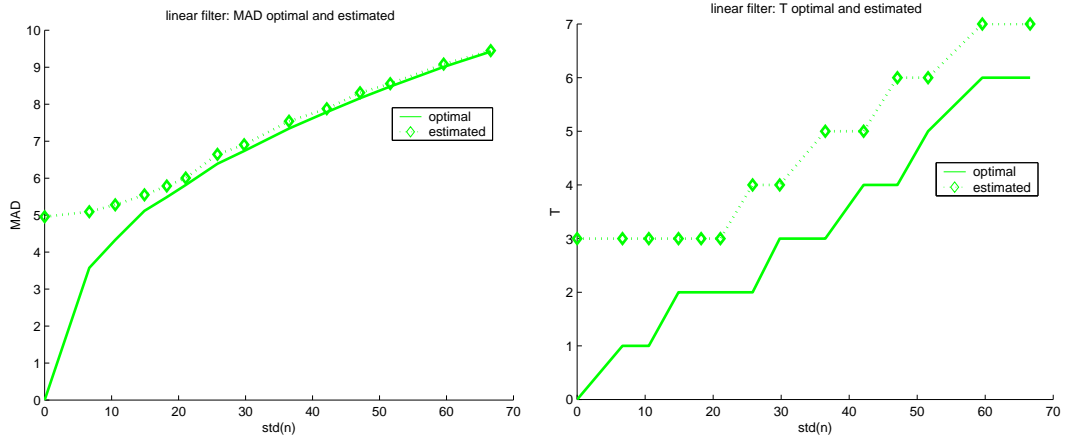
Figure 37: Experiment F, linear diffusion. Values of $MAD(\mathbf{u}(T) - \widetilde{\mathbf{f}})$ for the optimal and estimated time on the left; the optimal and estimated values of time T on the right.
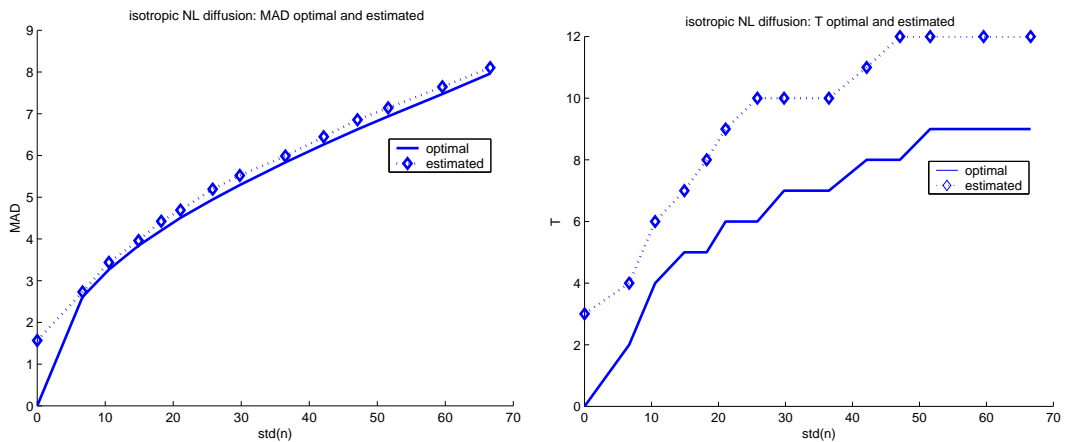
Figure 38: Experiment F, isotropic NL diffusion. Values of $MAD(\mathbf{u}(T) - \widetilde{\mathbf{f}})$ for the optimal and estimated time on the left; the optimal and estimated values of time T on the right.
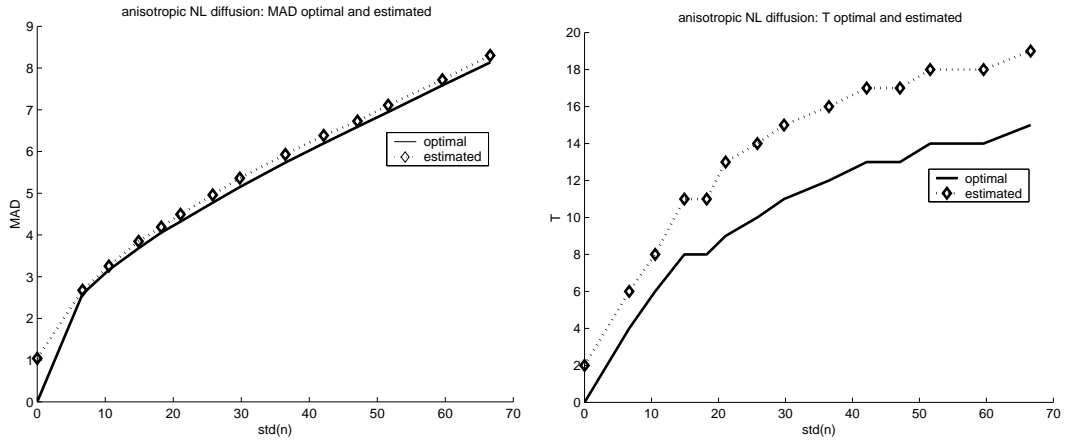
Figure 39: Experiment F, anisotropic NL diffusion. Values of $\mathrm{MAD}(\mathbf{u}(T) - \widetilde{\mathbf{f}})$ for the optimal and estimated time on the left; the optimal and estimated values of time T on the right.
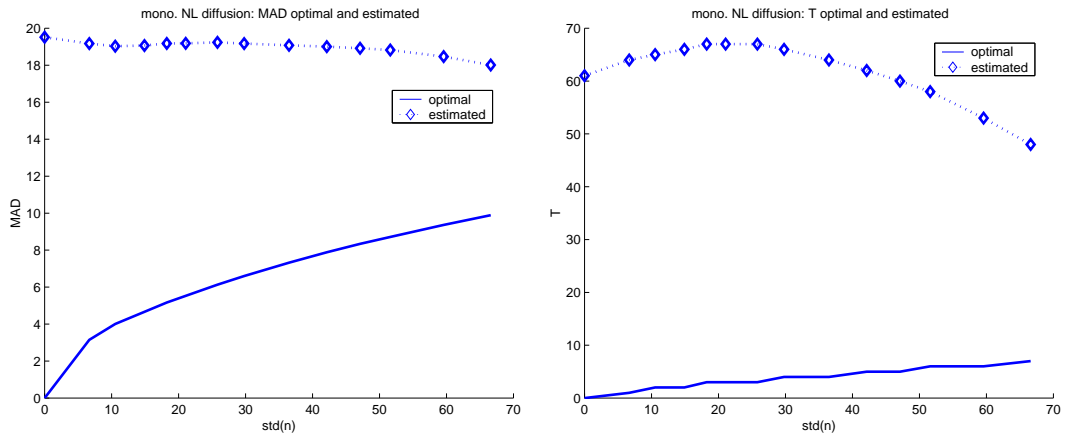
Figure 40: Experiment F, monotonicity-enhancing NL diffusion. Values of $\mathrm{MAD}(\mathbf{u}(T) - \widetilde{\mathbf{f}})$ for the optimal and estimated time on the left; the optimal and estimated values of time T on the right.
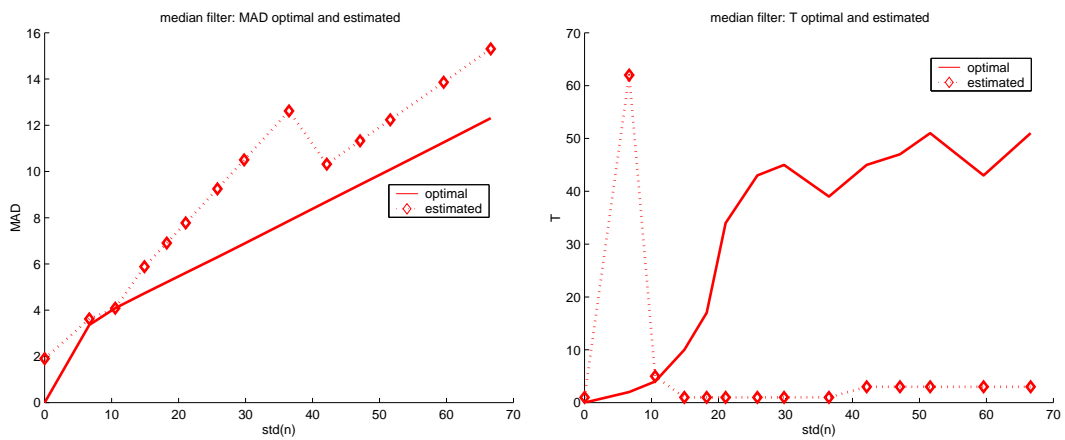
Figure 41: Experiment F, iterated median filter. Values of $\mathrm{MAD}(\mathbf{u}(T) - \widetilde{\mathbf{f}})$ for the optimal and estimated time on the left; the optimal and estimated values of time T on the right.

Figure 42: Some of the input images for Experiment G (size 433×437). From left to right, increasing amount of pixels was corrupted with salt&pepper noise: 0, 5, 20, 40, and 70 percent, respectively.

2.8 Experiment G
Salt and pepper noise, cymbidium image

Some of the input images for experiment G are seen in Fig. 42; it shows again the cymbidium image as in the previous section, but this time corrupted with salt&pepper noise. What results were obtained in this case (see Tables 13–14 and Figures 43–48):

- The value of the stopping time is overestimated for higher amounts of noise with the classical diffusion and iterated median filters; however, this error does not harm the filtered results much.

- The estimation does not work with monotonicity-enhancing NL diffusion.

- Salt-and-pepper noise is best removed by the median filter. In this experiment, we see for the first time that the estimated T (understood as number of iterations) for iterated median filtering is in good correspondence with the optimal values – or is it the other way round, and the optimal values here fit the unchanging estimates of T (at least for relatively smaller amount of noise)?

	linear diff.		iso. NL diff.		aniso. NL diff.		mono. NL diff.		iter. median	
$\mathrm{var}(n)$	T_{opt}	T_{corr}	T_{opt}	T_{corr}	T_{opt}	T_{corr}	T_{opt}	T_{corr}	T_{opt}	T_{corr}
0	0	3	0	3	0	2	0	61	0	1
206	0	3	0	6	0	22	0	67	0	1
534	0	4	0	18	0	29	0	72	1	1
1052	0	4	8	19	12	30	0	74	1	1
1583	2	5	7	19	11	26	3	60	1	1
2112	2	6	6	14	10	23	3	77	1	1
3180	3	7	7	25	9	20	3	82	1	2
4291	3	9	6	17	9	21	3	99	2	2
6357	3	12	5	16	8	26	4	28	2	2
8430	3	18	4	18	8	34	4	25	4	2
10464	4	26	4	22	8	43	4	28	8	2
12587	4	38	5	31	9	59	4	25	17	2
14669	5	62	5	47	10	98	100	13	28	2

Table 13: Optimal and estimated values of T for varied amount of noise and for various filtering methods in Experiment G.

	linear diff.		iso. NL diff.		aniso. NL diff.		mono. NL diff.		iter. median	
$\mathrm{var}(n)$	D_{opt}	D_{corr}	D_{opt}	D_{corr}	D_{opt}	D_{corr}	D_{opt}	D_{corr}	D_{opt}	D_{corr}
0	0.00	4.95	0.00	1.56	0.00	1.04	0.00	19.51	0.00	1.90
206	1.23	5.48	1.22	3.08	1.23	4.24	1.30	19.11	1.26	1.92
534	3.19	6.83	3.14	5.27	3.13	5.47	3.24	20.83	1.98	1.98
1052	6.28	8.09	6.34	6.87	6.21	7.08	6.47	20.43	2.07	2.07
1583	8.88	9.75	7.64	8.52	7.73	8.55	9.16	21.00	2.15	2.15
2112	10.42	11.47	9.49	10.07	9.26	10.12	10.87	21.91	2.27	2.27
3180	13.53	14.50	12.64	14.49	12.45	13.34	14.24	24.23	2.51	2.58
4291	16.68	17.95	15.67	17.20	15.80	17.08	17.43	28.81	2.70	2.70
6357	22.61	24.07	22.12	24.52	22.39	24.46	23.72	26.50	3.12	3.12
8430	28.83	30.67	28.36	30.67	29.03	31.22	29.39	31.86	3.73	4.24
10464	34.79	36.75	35.16	37.27	34.79	36.87	36.02	39.33	4.44	7.39
12587	41.37	43.33	41.33	43.43	41.19	43.18	42.11	45.19	6.23	15.67
14669	47.67	49.70	47.59	49.50	47.74	49.74	45.37	46.15	11.60	30.72

Table 14: Optimal and estimated values of $\mathrm{MAD}(\mathbf{u}(T) - \widetilde{\mathbf{f}})$ for varied amount of noise and for various filtering methods in Experiment G.
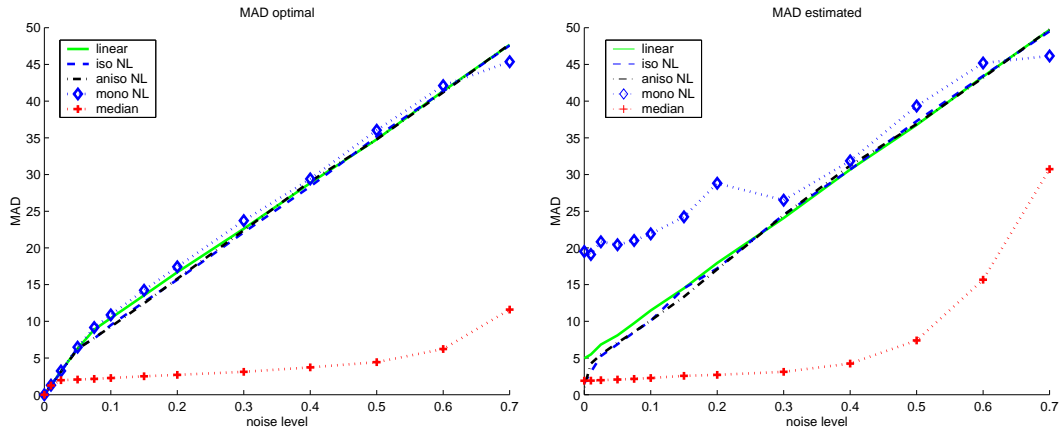
Figure 43: Experiment G. Plots of the error residual $MAD(\mathbf{u}(T) - \widetilde{\mathbf{f}})$ after filtering: optimal for each method and each noise level on the left, with estimated stopping time on the right.
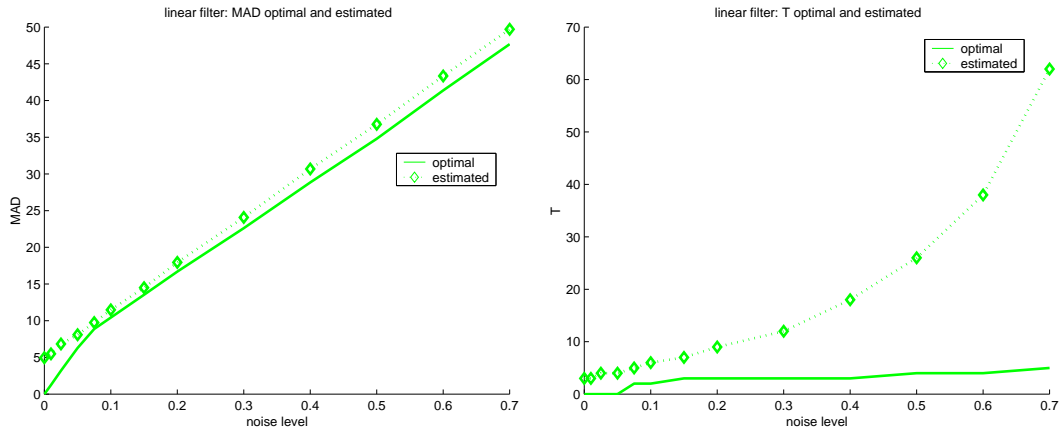
Figure 44: Experiment G, linear diffusion. Values of $MAD(\mathbf{u}(T) - \widetilde{\mathbf{f}})$ for the optimal and estimated time on the left; the optimal and estimated values of time T on the right.
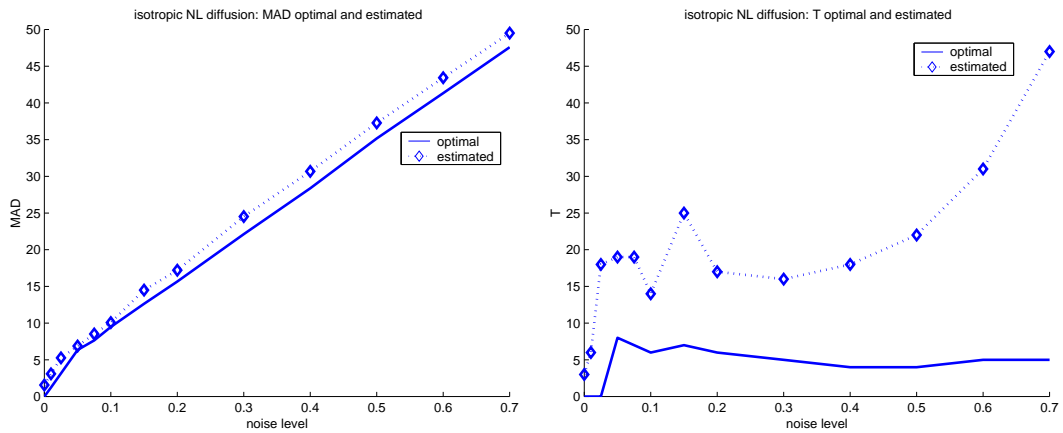
Figure 45: Experiment G, isotropic NL diffusion. Values of $MAD(\mathbf{u}(T) - \widetilde{\mathbf{f}})$ for the optimal and estimated time on the left; the optimal and estimated values of time T on the right.
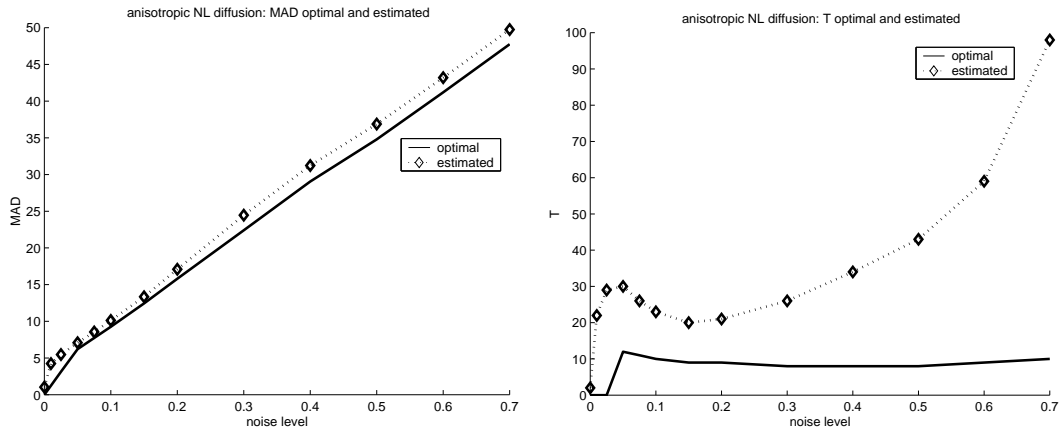
Figure 46: Experiment G, anisotropic NL diffusion. Values of $\mathrm{MAD}(\mathbf{u}(T)-\widetilde{\mathbf{f}})$ for the optimal and estimated time on the left; the optimal and estimated values of time T on the right.
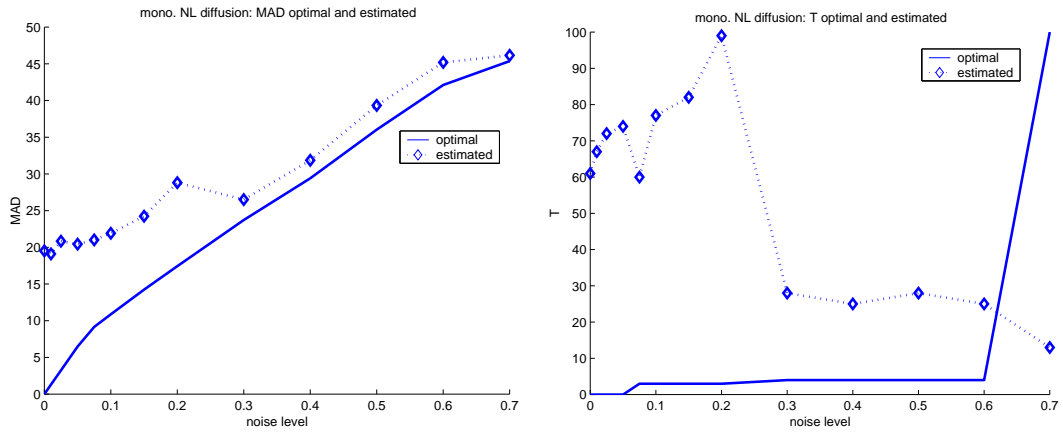
Figure 47: Experiment G, monotonicity-enhancing NL diffusion. Values of $\mathrm{MAD}(\mathbf{u}(T)-\widetilde{\mathbf{f}})$ for the optimal and estimated time on the left; the optimal and estimated values of time T on the right.
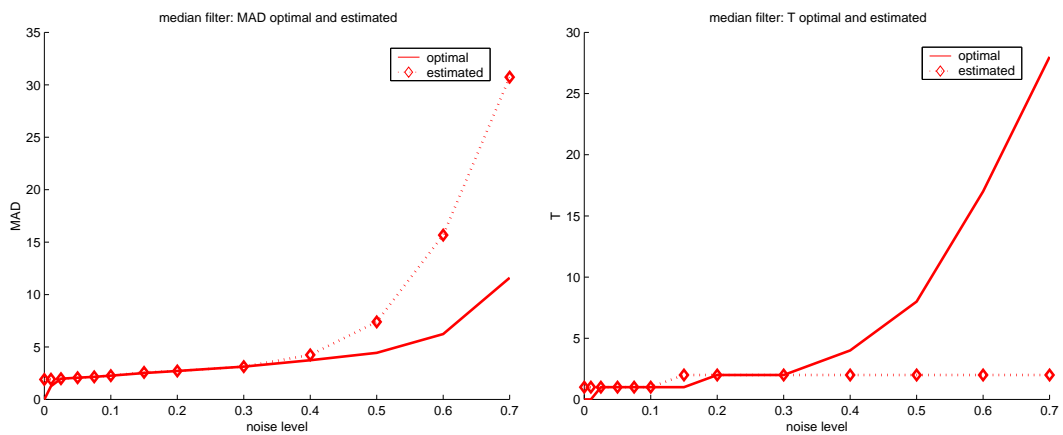
Figure 48: Experiment G, iterated median filter. Values of $\mathrm{MAD}(\mathbf{u}(T)-\widetilde{\mathbf{f}})$ for the optimal and estimated time on the left; the optimal and estimated values of time T on the right.
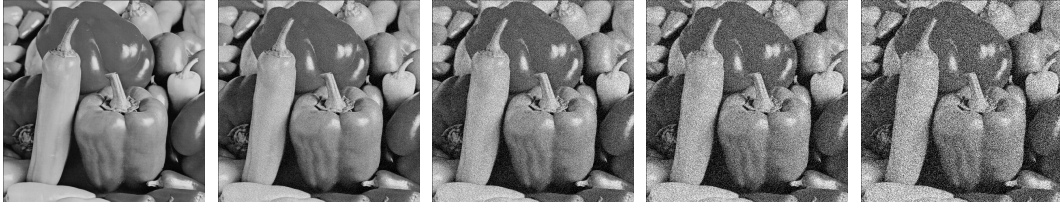
Figure 49: Some of the input images for Experiment H (size 433×437). From left to right, increasing amount of pixels was corrupted with salt&pepper noise: 0, 5, 20, 40, and 70 percent, respectively.

2.9 Experiment H
Gaussian noise, peppers image

In experiment H, we add Gaussian noise to the image of peppers; some of the input images are seen in Fig. 49. The results are presented in Tables 15–16 and Figures 50–55, and our comments will be brief:

- The decorrelation criterion gives very good estimates of the optimal stopping time for classical diffusion filters (linear, isotropic and anisotropic nonlinear).

- The estimation of T does not work with iterated median filtering and with monotonicity-enhancing NL diffusion.

- The isotropic and anisotropic NL diffusion yields the best filtering performance, both for the optimal and estimated stopping time T.

	linear diff.		iso. NL diff.		aniso. NL diff.		mono. NL diff.		iter. median	
var(n)	T_{opt}	T_{corr}	T_{opt}	T_{corr}	T_{opt}	T_{corr}	T_{opt}	T_{corr}	T_{opt}	T_{corr}
0	0	2	0	2	0	3	0	7	0	1
28	1	2	1	3	3	5	1	9	2	1
72	1	2	2	4	4	7	1	9	2	1
144	1	2	3	4	5	8	1	11	4	1
217	1	2	4	5	7	9	2	12	7	1
289	2	3	5	6	7	10	2	12	8	1
434	2	3	6	7	9	11	2	12	11	1
578	2	3	6	7	9	12	2	12	13	1
868	2	4	6	7	10	12	3	11	17	1
1157	3	4	7	8	11	14	3	10	21	1
1447	3	4	7	8	11	14	3	10	27	1
1736	3	5	7	8	11	14	4	10	27	1
2315	4	5	8	9	13	15	4	10	31	3
2894	4	6	8	9	13	16	4	10	32	3

Table 15: Optimal and estimated values of T for varied amount of noise and for various filtering methods in Experiment H.

	linear diff.		iso. NL diff.		aniso. NL diff.		mono. NL diff.		iter. median	
var(n)	D_{opt}	D_{corr}	D_{opt}	D_{corr}	D_{opt}	D_{corr}	D_{opt}	D_{corr}	D_{opt}	D_{corr}
0	0.00	4.94	0.00	2.23	0.00	2.08	0.00	8.99	0.00	2.74
28	3.94	5.05	3.05	3.21	2.85	3.08	3.65	10.58	3.63	3.69
72	4.37	5.20	3.71	3.83	3.50	3.73	4.15	10.49	4.15	4.42
144	4.97	5.42	4.21	4.26	4.02	4.18	4.87	11.80	4.72	5.34
217	5.49	5.64	4.55	4.60	4.33	4.44	5.39	12.50	5.11	6.10
289	5.83	6.31	4.82	4.87	4.55	4.65	5.69	12.82	5.42	6.76
434	6.20	6.53	5.21	5.25	4.90	4.95	6.20	12.91	5.94	7.89
578	6.53	6.74	5.47	5.51	5.20	5.30	6.66	13.47	6.39	8.87
868	7.13	7.39	5.90	5.92	5.68	5.74	7.29	13.23	7.14	10.53
1157	7.48	7.66	6.26	6.28	6.03	6.12	7.78	12.84	7.78	11.94
1447	7.81	7.91	6.56	6.59	6.39	6.48	8.26	13.13	8.34	13.20
1736	8.13	8.31	6.84	6.87	6.73	6.82	8.66	13.34	8.85	14.34
2315	8.59	8.67	7.30	7.33	7.21	7.28	9.29	13.88	9.75	11.59
2894	8.99	9.11	7.72	7.76	7.70	7.83	9.88	14.34	10.56	12.72

Table 16: Optimal and estimated values of $\text{MAD}(\mathbf{u}(T) - \widetilde{\mathbf{f}})$ for varied amount of noise and for various filtering methods in Experiment H.
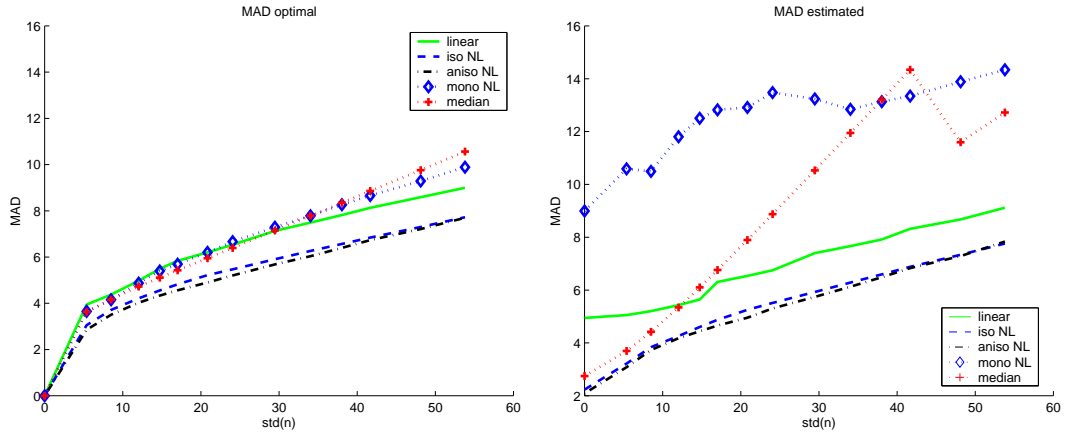
Figure 50: Experiment H. Plots of the error residual $MAD(\mathbf{u}(T) - \widetilde{\mathbf{f}})$ after filtering: optimal for each method and each noise level on the left, with estimated stopping time on the right.
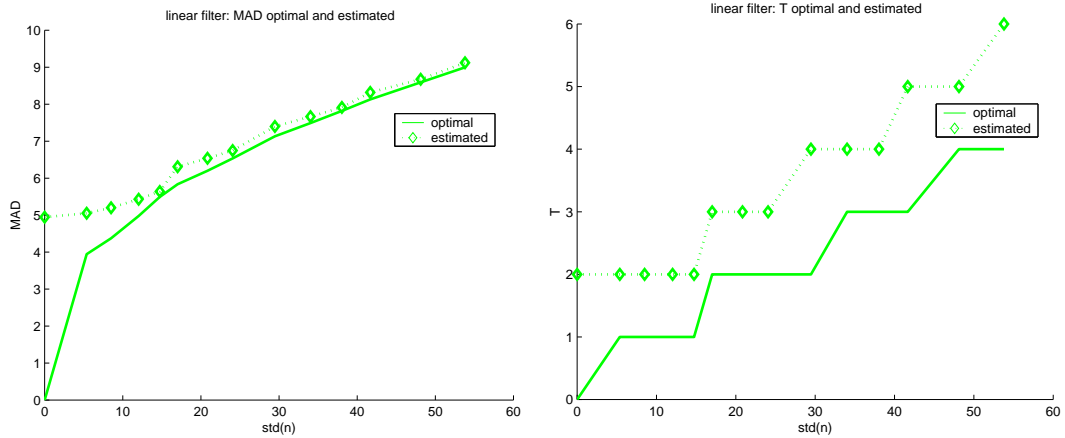
Figure 51: Experiment H, linear diffusion. Values of $\mathrm{MAD}(\mathbf{u}(T) - \widetilde{\mathbf{f}})$ for the optimal and estimated time on the left; the optimal and estimated values of time T on the right.
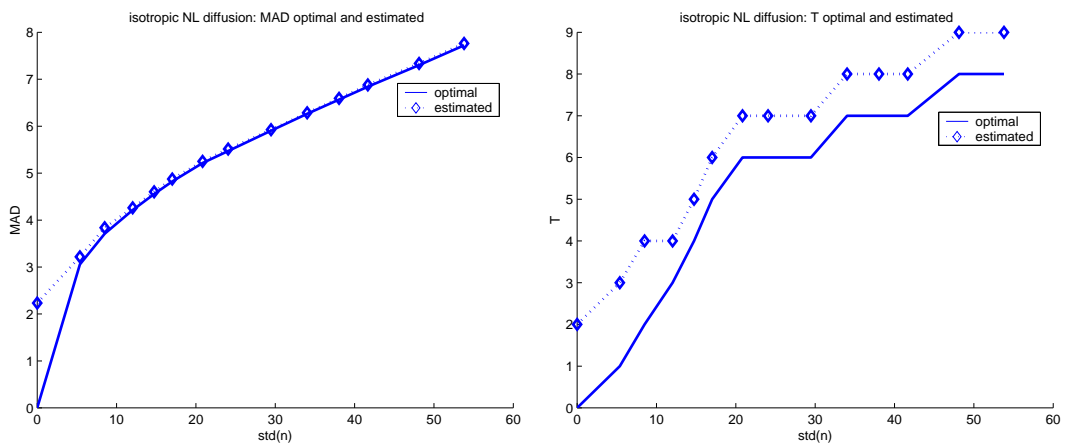
Figure 52: Experiment H, isotropic NL diffusion. Values of $\mathrm{MAD}(\mathbf{u}(T) - \widetilde{\mathbf{f}})$ for the optimal and estimated time on the left; the optimal and estimated values of time T on the right.
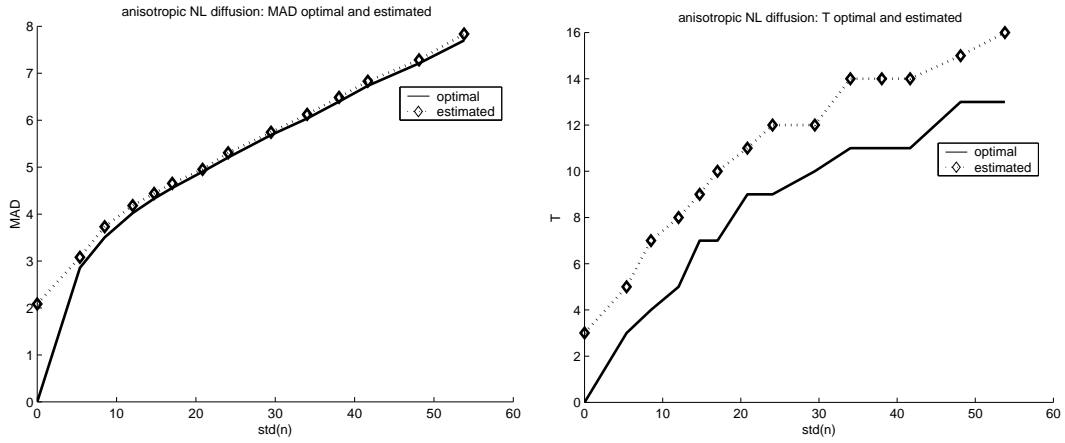
Figure 53: Experiment H, anisotropic NL diffusion. Values of $\mathrm{MAD}(\mathbf{u}(T) - \widetilde{\mathbf{f}})$ for the optimal and estimated time on the left; the optimal and estimated values of time T on the right.
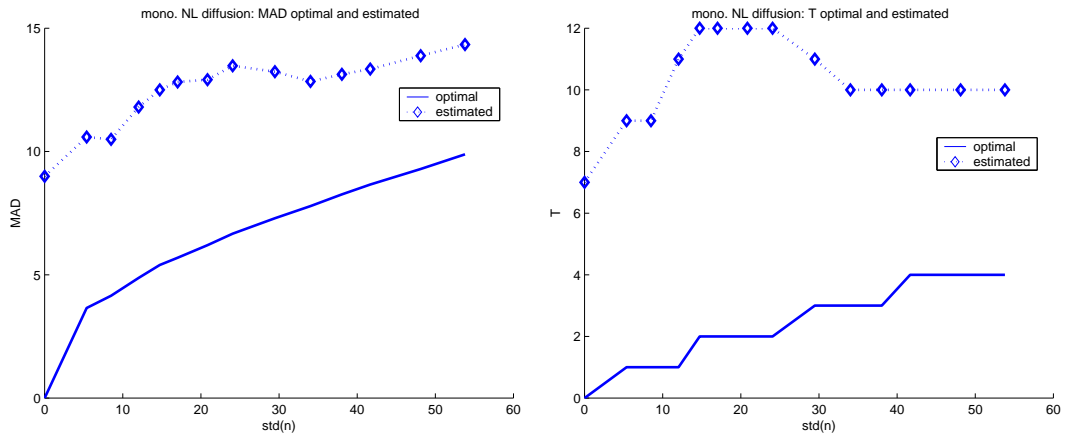
Figure 54: Experiment H, monotonicity-enhancing NL diffusion. Values of $\mathrm{MAD}(\mathbf{u}(T) - \widetilde{\mathbf{f}})$ for the optimal and estimated time on the left; the optimal and estimated values of time T on the right.
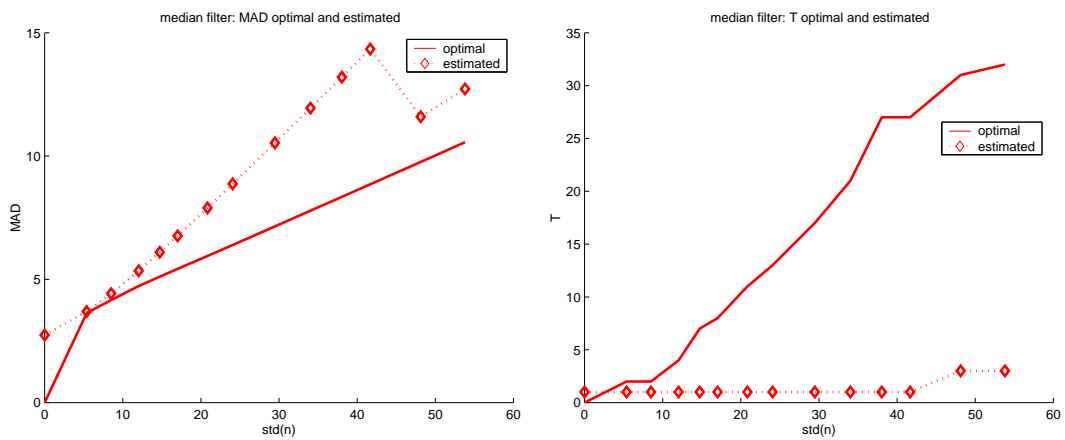
Figure 55: Experiment H, iterated median filter. Values of $\mathrm{MAD}(\mathbf{u}(T) - \widetilde{\mathbf{f}})$ for the optimal and estimated time on the left; the optimal and estimated values of time T on the right.

experiment	$T_{\mathrm{corr}}/T_{\mathrm{opt}}$				
	linear diff.	iso. NL diff.	aniso NL diff.	mono NL diff.	iter. median
A	1	1	1	1.15	0.07
B	0.71	0.43	0.44	0.8	0.04
C	1.28	0.3	0.65	10.79	0.03
D	0.76	0.72	0.87	1.68	0.12
E	76.32	7.74	2.13	43.01	0.44
F	1.68	1.49	1.35	21.44	2.53
G	5.47	4.26	4.09	14.74	0.81
H	1.66	1.38	1.36	5.45	0.16

Table 17: Ratios between correlation-estimated and optimal stopping times, $T_{\mathrm{corr}}/T_{\mathrm{opt}}$, averaged for each combination of test image and filtering method across all noise levels. The noise was additive Gaussian in the range of SNR $\in [1, \infty)$ except for experiment G, for which 0–70 per cent of pixels were corrupted with salt&pepper noise.

experiment	$D_{\mathrm{corr}}/D_{\mathrm{opt}}$				
	linear diff.	iso. NL diff.	aniso NL diff.	mono NL diff.	iter. median
A	1	1	1	1.01	1.39
B	1.02	1.59	1.19	1.04	1.76
C	1.03	1.52	1.08	2.6	1.74
D	1.02	1.06	1.01	1.08	1.36
E	2.97	1.36	1.18	3.15	1.14
F	1.07	1.04	1.03	3.18	1.29
G	1.46	1.25	1.33	3.11	1.38
H	1.07	1.01	1.03	2	1.31

Table 18: Relative filtering quality $D_{\mathrm{corr}}/D_{\mathrm{opt}}$ computed as a ratio between the filtering residuals $\mathrm{MAD}\big(\mathbf{u}(T) - \widetilde{\mathbf{f}}\big)$ at the correlation-estimated and optimal stopping times T, averaged for each image and filtering method across all noise levels.

2.10 Summary of experiments A–H

In experiments A–H we corrupted original images with either Gaussian or salt&pepper noise artificially, filtered the signal using several methods, and compared the optimal and correlation–estimated stopping time for each of them. The numerical measurements are summarized in Tables 17–20.

The values of the ratio $T_{\mathrm{corr}}/T_{\mathrm{opt}}$, averaged for each test image and each filter type across all noise levels, are given in Table 17. Table 18 presents the corresponding average relative filtering quality

$$\frac{D_{\mathrm{corr}}}{D_{\mathrm{opt}}} = \frac{\mathrm{MAD}\big(\mathbf{u}(T_{\mathrm{corr}}) - \widetilde{\mathbf{f}}\big)}{\mathrm{MAD}\big(\mathbf{u}(T_{\mathrm{opt}}) - \widetilde{\mathbf{f}}\big)}. \tag{3}$$

Similar measurements, but presented for each noise level with averaged contribution of individual images, are given in Tables 19 and 20.

You can see in Tables 17–20 that the estimation of the stopping time T using the decorrelation criterion (2) gives usually good results for linear, isotropic and anisotropic NL diffusion, where the values of T_{corr} lie in most cases in the range $[0.5T_{\mathrm{opt}}, 2T_{\mathrm{opt}}]$ (more precisely, the estimated values lie in this range in 68, 56, and 71 percent of all experiments for linear, isotropic and anisotropic diffusion, respectively). The estimation results are more reliable when there is a higher amount of noise in the input image.

The errors in the estimation of T lead usually to only small relative decay in the filtering performance compared to the optimal results: the relative error is smaller than 20 percent

SNR	$T_{\text{corr}}/T_{\text{opt}}$				
	linear diff.	iso. NL diff.	aniso NL diff.	mono NL diff.	iter. median
100	1.58	5.55	1.36	18.92	5.35
40	1.61	3.43	1.2	18.67	0.44
20	15.31	2.68	1.17	17.62	0.22
13.33	15.32	2	1.16	15.23	0.19
10	15.29	1.46	1.1	14.97	0.12
6.67	15.35	1.29	1.04	14.76	0.11
5	15.17	1.13	1.08	13.6	0.08
3.33	15.28	1.15	1.05	8.28	0.07
2.5	7.99	1.21	1.08	7.5	0.07
2	7.81	1.14	1.06	7.25	0.08
1.67	7.75	1.13	1.08	6.58	0.07
1.25	7.58	1.08	1.06	5.13	0.09
1	7.5	0.99	1.07	4.68	0.08

Table 19: Ratios between correlation-estimated and optimal stopping times, $T_{\text{corr}}/T_{\text{opt}}$, averaged for each combination of noise level and filtering method across all test images.

SNR	$D_{\text{corr}}/D_{\text{opt}}$				
	linear diff.	iso. NL diff.	aniso NL diff.	mono NL diff.	iter. median
100	1.87	1.49	1.14	3.36	1.37
40	1.49	1.38	1.09	2.76	1.36
20	1.39	1.29	1.07	2.46	1.42
13.33	1.34	1.27	1.07	2.29	1.45
10	1.33	1.23	1.07	2.16	1.47
6.67	1.29	1.2	1.06	1.98	1.51
5	1.26	1.21	1.07	1.86	1.54
3.33	1.22	1.16	1.07	1.71	1.58
2.5	1.19	1.12	1.07	1.62	1.45
2	1.18	1.13	1.07	1.55	1.39
1.67	1.17	1.1	1.06	1.52	1.41
1.25	1.15	1.19	1.05	1.45	1.28
1	1.14	1.15	1.05	1.4	1.29

Table 20: Relative filtering quality $D_{\text{corr}}/D_{\text{opt}}$ computed as a ratio between the filtering residuals $\text{MAD}\big(\mathbf{u}(T) - \widetilde{\mathbf{f}}\big)$ at the correlation-estimated and optimal stopping times T, averaged for each combination of noise level and filtering method across all test images.

in 93 percent of experiments with the anisotropic NL diffusion filter, in 86 percent of experiments with the linear diffusion, and in 71 percent of experiments with the isotropic NL diffusion filtering. Note also that this higher error with isotropic NL diffusion is only relative to the optimal values, the absolute results of isotropic NL filter with estimated stopping time outperform other methods in most cases.

The estimation works well with linear diffusion except the MRI data (Experiment E). On the other hand, the minimum of the signal-noise correlation does not lead to near-optimal stopping times with monotonicity-ehnancing NL diffusion and with iterated median filters, perhaps with the exception of the data suited directly for these types of filters (i.e. the piecewise linear function, Experiment D, and the salt&pepper noise in Experiment G, respectively). This worse performance may be caused by the fact that unlike classical diffusion filters which create information-reducing scale-spaces and observe the maximum-minimum principle, monotonicity-enhancing diffusion and iterated median filter often form a solution for which the correlation $\mathrm{corr}\big(\mathbf{u}(0) - \mathbf{u}(t), \mathbf{u}(t)\big)$ changes its sign into negative values. Also, the median filtering does not preserve the average grey level of the image, which was one of the theoretical assumptions on the filtering methods.

2.11 Experiment I: Comparison between correlation– and SNR–estimated stopping time

Another example of the experimental performance of the decorrelation criterion is seen in Figures 56 and 57, measured on cymbidium data (Fig. 3f) with varied amount of additive Gaussian noise combined with an anisotropic NL diffusion filter. The former figure compares three stopping times: the optimal T_{opt}, T_{SNR} determined using the knowledge on the signal-to-noise ratio in the input image [10], and our decorrelation-estimated T_{corr}. All alternative stopping times are computed for a series of input images with varied amount of noise present; the standard deviation of noise in the input data is represented by the horizontal axis of the graphs. While the SNR method easily underestimates or overestimates the optimal stopping time (depending on the amount of noise in the input data), the correlation minimization leads to near-optimal results for all noise levels. The three graphs are plotted for iteration time steps $\tau \in \{0.1, 0.5, 1\}$.

The actually obtained quality measure $\mathrm{MAD}(\mathbf{u}(T) - \widetilde{\mathbf{f}})$ is shown in Fig. 57, this time with $\tau = 0.5$. You can see that for all noise levels the correlation-estimated time leads to filtering results very close to the optimal values obtainable by the nonlinear diffusion.
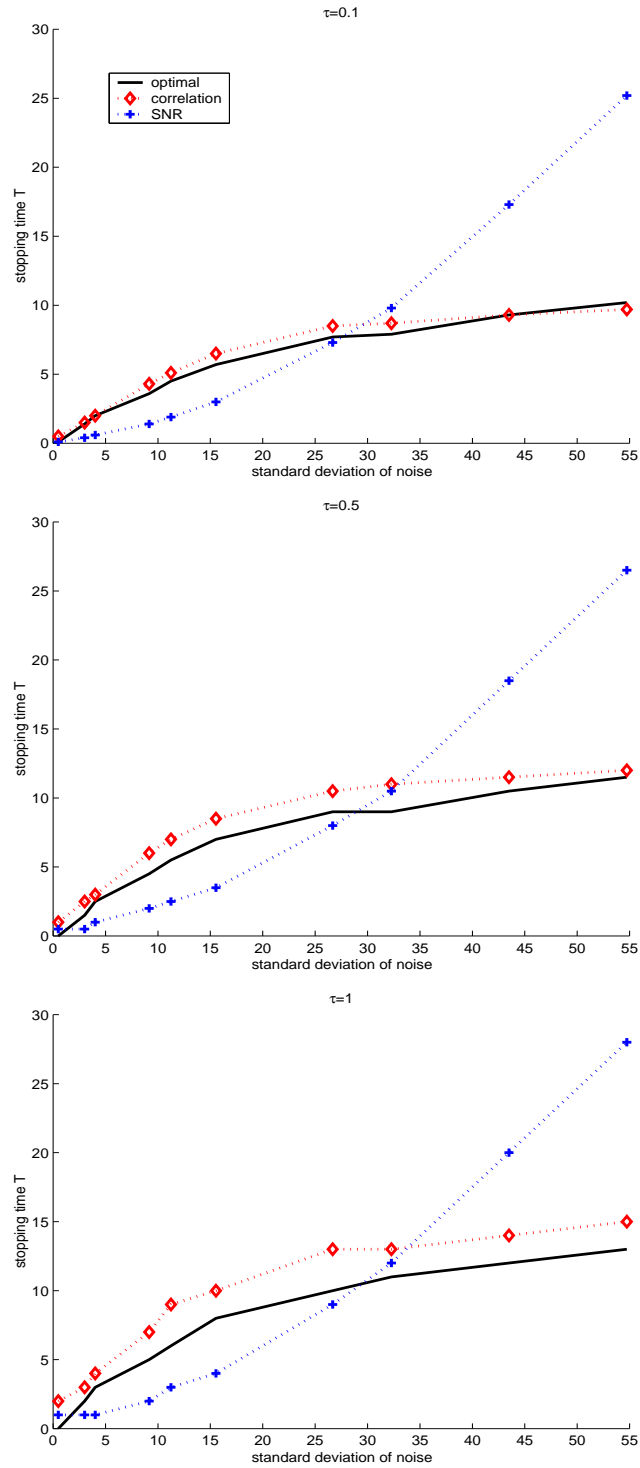
Figure 56: The stopping time T_{SNR} determined by the SNR method (dotted with crosses), and T_{corr} obtained through the covariance minimization (dotted with diamonds) compared to the optimal stopping time T_{opt} (solid line). The graphs are plotted against the standard deviation of noise in the input image; the three figures represent the same measurements for different iteration time-step sizes (top to bottom): $\tau = 0.1$, $\tau = 0.5$, $\tau = 1$.
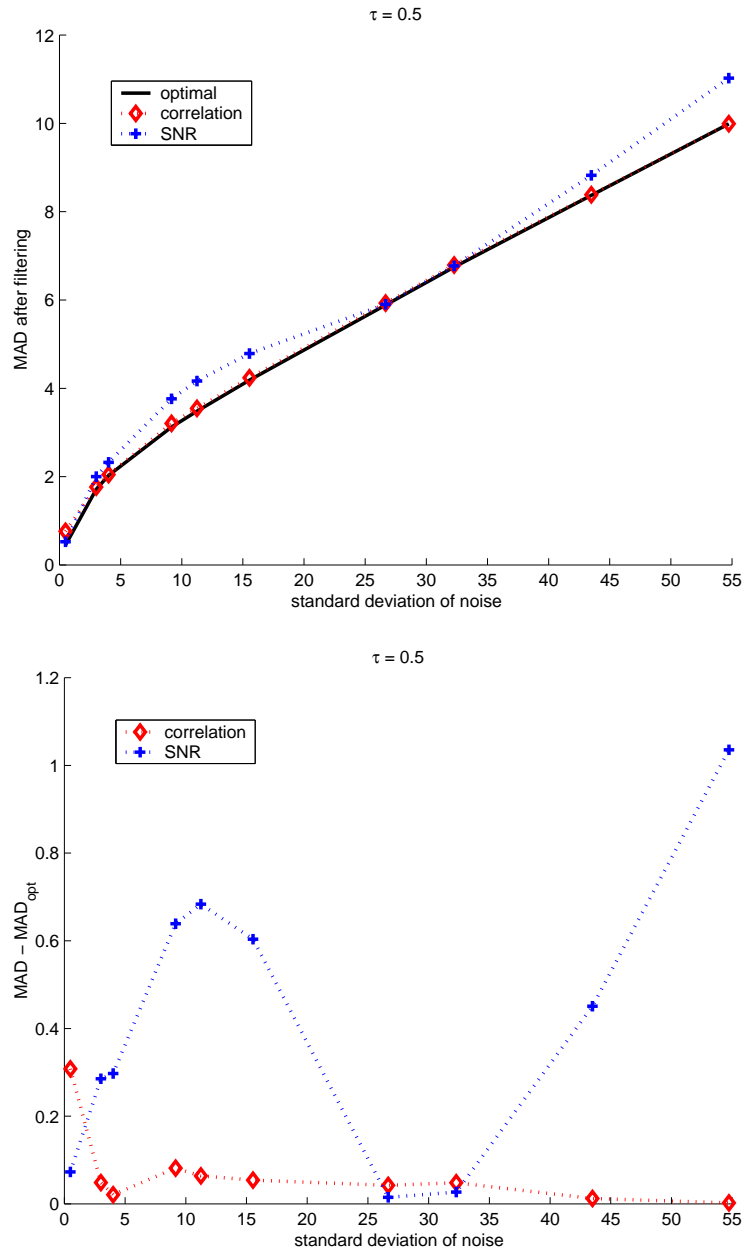
Figure 57: Top: the MAD distance of the filtered data from the ideal noise-free image, $\mathrm{MAD}(\mathbf{u}(T) - \widetilde{\mathbf{f}})$, using the SNR and the correlation-minimization time selection strategies. Bottom: the difference between the estimated result and the optimal one, $\mathrm{MAD}(\mathbf{u}(T) - \mathbf{u}(T_{\mathrm{opt}}))$.

2.12 Experiment J
Can correlation help to choose the filtering method?

So far, we have been addressing the problem of selecting a good stopping time T from a sequence of iterations. However, the correlation between the filtered signal and the filtering noise $\text{corr}\big(\mathbf{u}(0) - \mathbf{u}(t), \mathbf{u}(t)\big)$ carries more information on the filtering process and can be exploited further: to estimate the filtering quality, to select parameters of the filtering process, or choose between several alternative filtering methods.

Let us return for a moment to Fig. 2. At the beginning of the diffusion filtering, the correlation coefficient declines fast until it reaches its minimum. If for some data the graph behaves differently, it may serve as a hint on some problems. As an example, we observed that if there is only a small amount of noise in the input image, the correlation $\text{corr}\big(\mathbf{u}(0) - \mathbf{u}(t), \mathbf{u}(t)\big)$ might grow from the first iterations. In such a case, the iteration time step τ has to be decreased adaptively and the diffusion restarted from time $t = 0$ until the correlation plot exhibits a clear minimum.

At its minimum, the term $\big|\text{corr}\big(\mathbf{u}(0) - \mathbf{u}(t), \mathbf{u}(t)\big)\big|$ measures the residual correlation between the filtered signal and the filtering noise. It can be also understood as a measure of filtering quality obtained by a particular filter with a given set of parameters; hopefully, a smaller residual correlation corresponds to a better filtering quality (the correlation is zero for the ideal filter). Then, the minimum of $\big|\text{corr}\big(\mathbf{u}(0) - \mathbf{u}(t), \mathbf{u}(t)\big)\big|$ can be used to compare the outputs of different filters or of one filter with different parameters, and may help us choose the best filter for the given input data.

As an initial attempt in this direction, we compare the filtering quality of three diffusion filters (linear, isotropic and anisotropic) with the residual signal–noise correlation in Figure 58. It shows the result obtained in all experiments A–H seen so far, for each of them starting with the smallest amount of noise on the left. You can see first that while the graph of the distance $\text{MAD}(\mathbf{u}(T) - \widetilde{\mathbf{f}})$ naturally increases with the amount of noise, the residual correlation $\big|\text{corr}\big(\mathbf{u}(0) - \mathbf{u}(T), \mathbf{u}(T)\big)\big|$ decreases. This is caused by the normalization with noise variance in the computation of correlation. However, what interests us is the relative order of the values of the filtering quality and the correlation between individual filters in each experiment. In Fig. 58, it is seen that this ordering mostly holds, and if not, the difference in the filtering quality is very small. Therefore we conclude that the minimum of $\big|\text{corr}\big(\mathbf{u}(0) - \mathbf{u}(t), \mathbf{u}(t)\big)\big|$ might help us decide on the best filter from linear, isotropic and anisotropic NL diffusion, alhough it would result in selecting isotropic NL diffusion in most of the cases seen so far.

In the second experiment, we try to select the best filter for a particular input from classical and monotonicity-enhancing anisotropic NL diffusion. We should assume that piecewise constant data are best filtered using the classical diffusion, while monotonicity-anhancing procedure is better suited for piecewise linear data. Figure 59 shows that the residual correlation may be used to select the better of the two filters only with care: it works fine for the data of Experiment B (indicating that classical diffusion with piecewise constant model should be employed), feasibly in Experiment D (prefering piecewise linear model of the monotonicity-enhancing procedure for piecewise linear data, although the decision does not correspond completely to the MAD distance between filtered output of the two method and the ideal data), but suggests an obsolete solution for the piecewise constant data of Experiment C. The reason for the latter failure can be perhaps blaimed on the fact that the monotonicity-enhancing procedure leads to results where the correlation $\text{corr}\big(\mathbf{u}(0) - \mathbf{u}(t), \mathbf{u}(t)\big)$ is negative; then, the time T estimated from the minimum of its absolute value is less stable and reliable than in the cases where the correlation does not change its sign (such as is the case with classical diffusion filters).

In the third experiment testing the validity of the idea that residual correlation might contribute to the selection or tuning of the restoration method, we filter the cymbidium
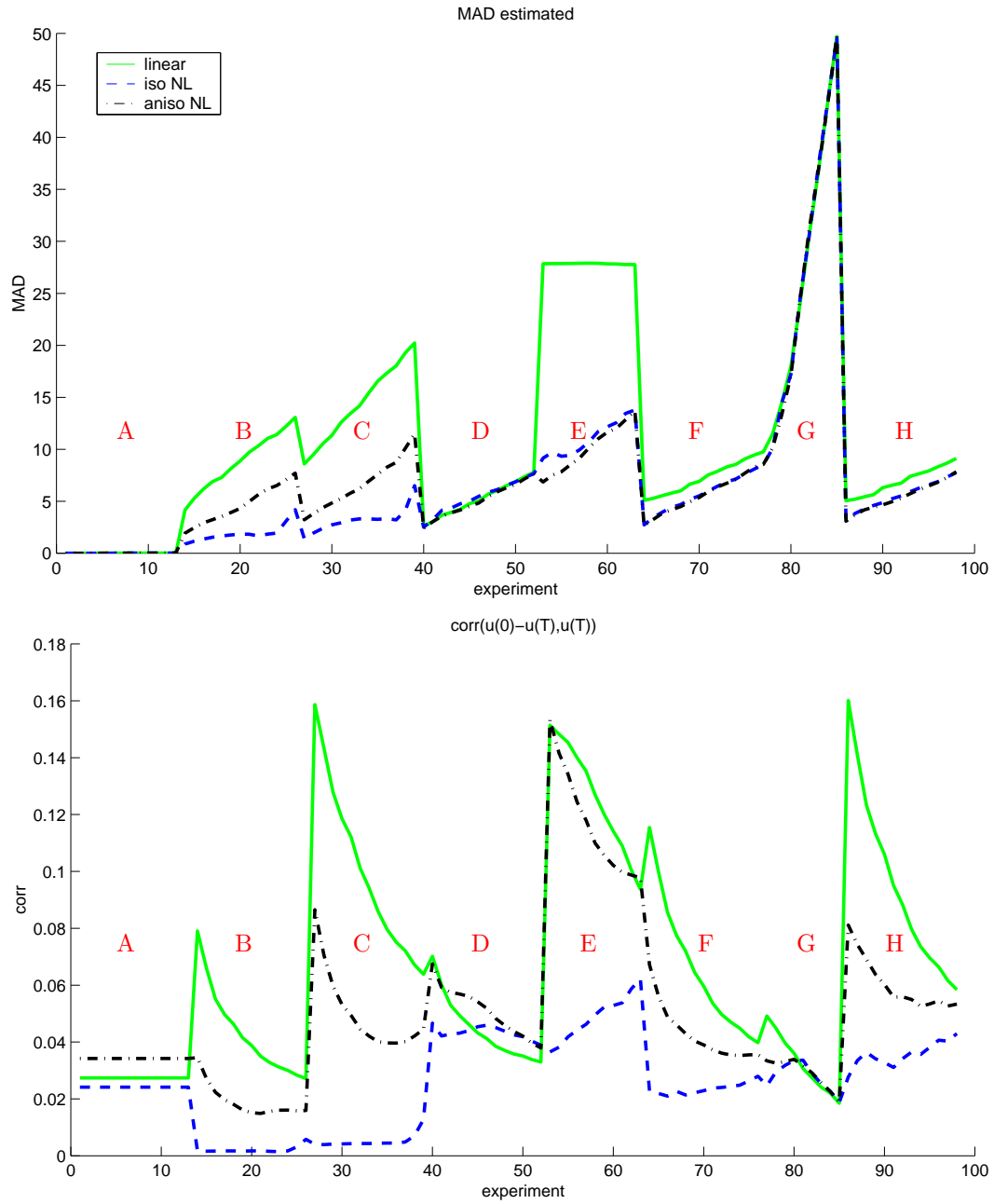
Figure 58: Correspondence between the residual signal-to-noise correlation and the filtering quality with linear, isotropic and anisotropic NL diffusion filter.
Top: quality of the filtering solution, measured by $\mathrm{MAD}(\mathbf{u}(T) - \widetilde{\mathbf{f}})$ at the time T determined using the decorrelation criterion, for all inputs of Experiments A–H.
Bottom: the corresponding value $\left|\mathrm{corr}\big(\mathbf{u}(0) - \mathbf{u}(T), \mathbf{u}(T)\big)\right|$.
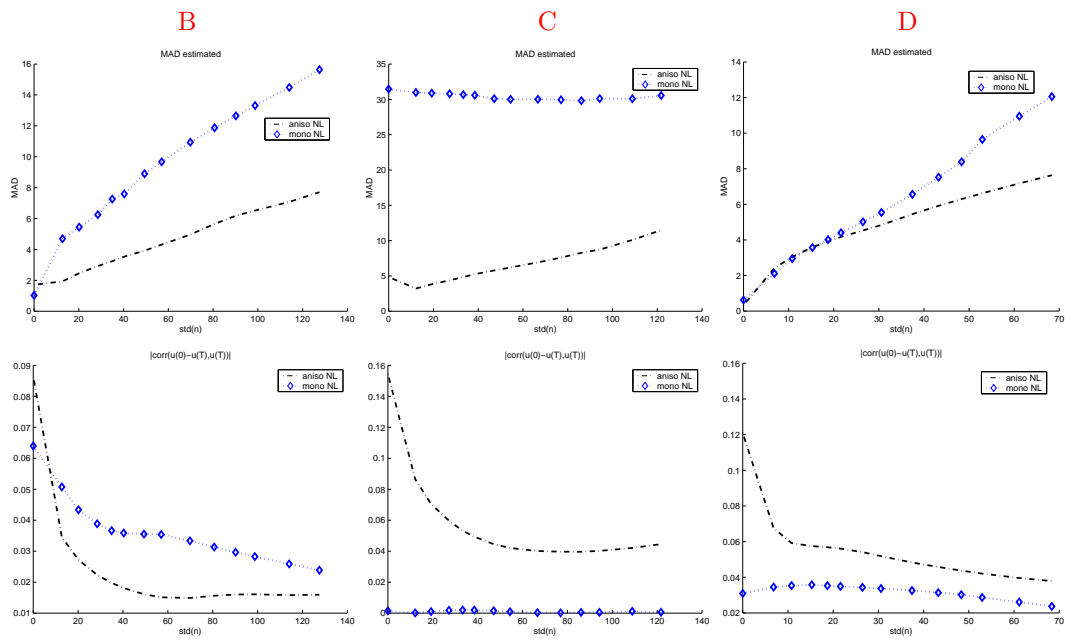
Figure 59: Can the residual correlation $|\operatorname{corr}\big(\mathbf{u}(0) - \mathbf{u}(T), \mathbf{u}(T)\big)|$ select the best model for the input data? Top: quality of the filtering solution, measured by $\operatorname{MAD}(\mathbf{u}(T) - \widetilde{\mathbf{f}})$ at the time T determined using the decorrelation criterion. Bottom: the corresponding value $|\operatorname{corr}\big(\mathbf{u}(0) - \mathbf{u}(T), \mathbf{u}(T)\big)|$. The input data were (left to right) those of Experiments B, C, and D, respectively. The plots compare results of classical anisotropic diffusion (using a piecewise constant model) and monotonicity-enhancing diffusion (piecewise linear model).
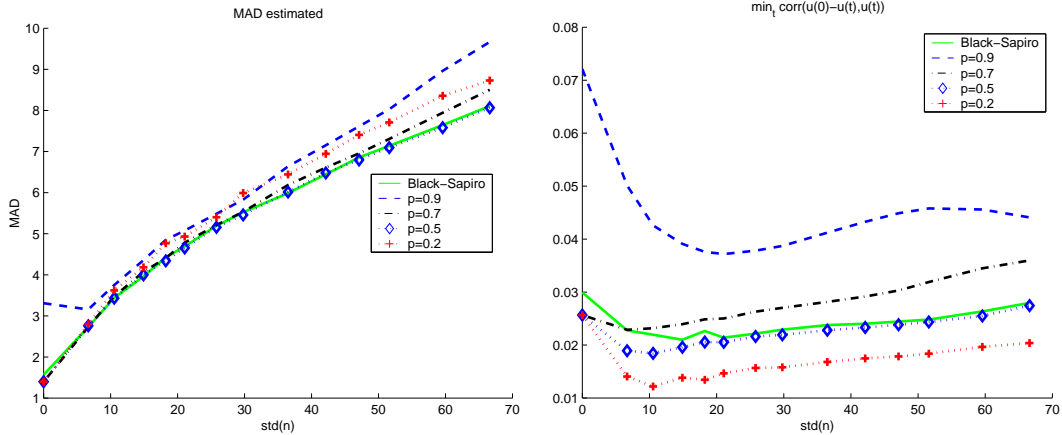
Figure 60: Comparison of filtering results obtained on the cymbidium image with varied amount of noise using a single type of filter (isotropic NL diffusion), but varying the parameter p which influences the computation of λ. Left: $\mathrm{MAD}(\mathbf{u}(T) - \widetilde{\mathbf{f}})$; right: $|\mathrm{corr}(\mathbf{u}(0) - \mathbf{u}(T), \mathbf{u}(T))|$. The graphs are plotted for p=0, 0.2, 0.5, 0.7 and 0.9.

image with Gaussian noise using isotropic NL diffusion, and vary the parameter λ which serves as a threshold determining how strong edges should be preserved in the diffusion process. More precisely, we vary the method which estimates the parameter λ from the input image, or its parameter p. For $p = 0$, the value of λ is estimated using the method of Black and Sapiro [1] from statistical properties of the image; for $p \in (0, 1)$, we set the parameter λ equal to a $100 \cdot p$ percentile of image gradients as proposed by Perona and Malik in [8].

The results are shown in Figures 60–61. The former presents results for several values of p and varied amount of noise in the input image; at each noise level, we would like the graphs of MAD and correlation to be in the same ordering, which, as you can see, is not exactly the case. The letter figure compares the filtering quality and correlation for one noise level only, and it is visible that the minimum of the MAD distance from the ideal solution does not coincide well with the minimum of the residual signal–noise correlation. While the correlation is minimised around $p = 0.2$, the optimal filtering performance is obtained if we either estimate λ using the method of Black and Sapiro, or employ the Perona–Malik procedure but with $p = 0.5$.[3]

---

[3]We should also remark that the Perona–Malik's idea to set λ to a $100 \cdot p$ percentile of image gradients is often used with $p = 0.9$, so that only 10 percent of strongest edges are preserved. Our experiments here would suggest a smaller value of p; however, it also depends on whether the percentile of gradients is recomputed in each step (which, due to gradients attenuated by the diffusion slows down the smoothing and combines well with a higher p), or whether we compute λ in the first step only, which was our choice here.
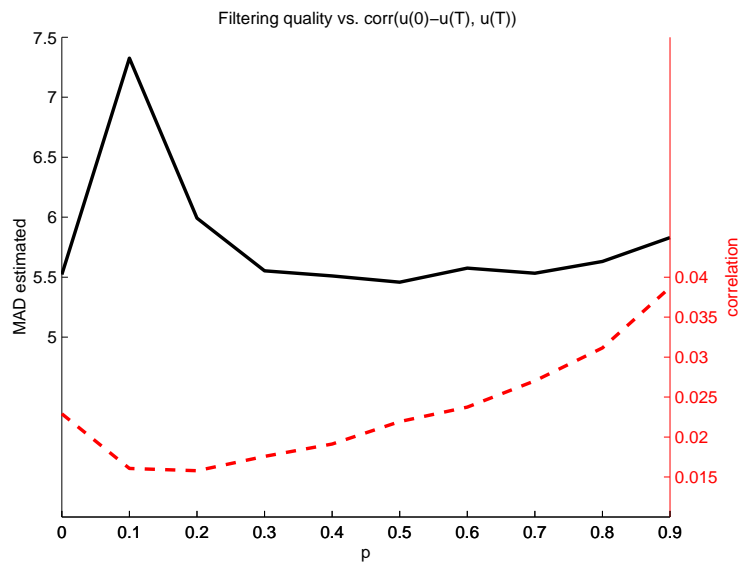
Figure 61: Graphs of $\mathrm{MAD}(\mathbf{u}(T) - \widetilde{\mathbf{f}})$ and $|\operatorname{corr}(\mathbf{u}(0) - \mathbf{u}(T), \mathbf{u}(T))|$ plotted for a single input image (cymbidium, SNR=5) with variable parameter p. For $p = 0$, the diffusivity parameter λ is estimated using the Black-Sapiro procedure [1]; in other cases, we set λ equal to a $100 \cdot p$ percentile of image gradients in the spirit of Perona and Malik's [8].

Figure 62: Noisy input image for the experiment in Figure 63.

2.13 Some filtered images

In this section, we show some images obtained using diffusion filtering combined with autonomous stopping time selection using the decorrelation criterion (2).

2.13.1 Triangle and rectangle

The first example compares the results of different diffusion algorithms filtering an originally black and white image with non-Gaussian additive noise. The input data are shown in Fig. 62: the noisy image was obtained by adding noise of uniform distribution in the range $[-255, 255]$ to the ideal input (Fig. 3c), and by restricting the noisy values into the interval $[0, 255]$.

In Fig. 63, the noise is smoothed by linear diffusion, isotropic nonlinear diffusion, and two anisotropic diffusion filters; the grey-values are stretched to the whole interval $[0, 255]$ so that a higher contrast between the dark and bright regions corresponds to a better noise-filtering performance. In all cases, the stopping time was determined autonomously by the signal–noise decorrelation criterion (2). You can see that in all cases, although quite different filtering algorithms were employed, the stopping criterion leads to results where most of the noise is removed and the ideal signal becomes apparent or suitable for further processing; we support this statement by showing the thresholded content of the filtered images in Fig. 64.

The stopping criterion was designed to minimize the distance between the ideal and filtered function. If visual quality was the goal to be achieved, we would probably stop the diffusion later, especially as linear diffusion (Fig. 63a) and the Weickert's edge-enhancing anisotropic diffusion [9] with maximum amount of diffusion in the coherence direction ($\varphi_2 = 1$, Fig. 63c) are concerned. We find however that the MAD distance and visual quality are in a good agreement in Fig. 63d which represents the result of the edge-enhancing diffusion with a smaller amount of diffusion in the coherence direction, $\varphi_2 = 0.2$ (see the thesis [6] for details on the filtering procedures).

2.13.2 Cymbidium experiment

Noise of normal distribution was added to the image of a cymbidium flower (Figure 65 top, courtesy of Michal Haindl), the noisy image was subjected to anisotropic diffusion filtering algorithm with the parameters $\sigma = 1$, $\tau = 0.5$, $\varphi_2 = 0.2$.[4] The optimal values for

---

[4]Briefly, σ is a parameter to regularize the estimation of image gradient from noisy discrete data, τ the iteration time step, φ_2 the amount of diffusion in the direction of maximum coherence, and λ a threshold determining how weak edges to smooth and how strong edges to preserve; details can be found in the thesis [6].
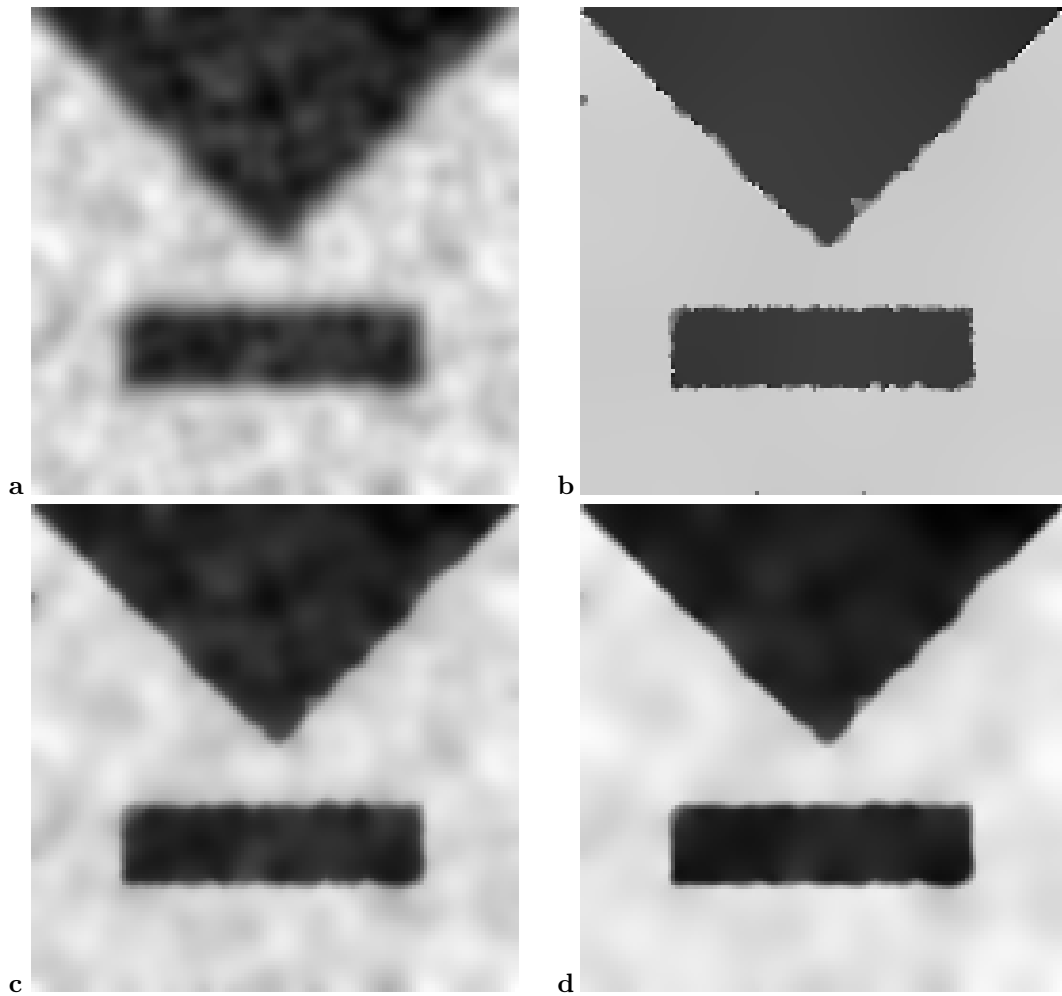
Figure 63: Comparing the different diffusion algorithms on the noisy data of Fig. 62, all with the stopping time selected autonomously using the decorrelation criterion: (a) linear diffusion, $T = 3.8$; (b) isotropic nonlinear diffusion, $T = 125$; (c) anisotropic NL diffusion, $\varphi_2 = 1$, $T = 15$; (d) anisotropic NL diffusion, $\varphi_2 = 0.2$, $T = 32$.
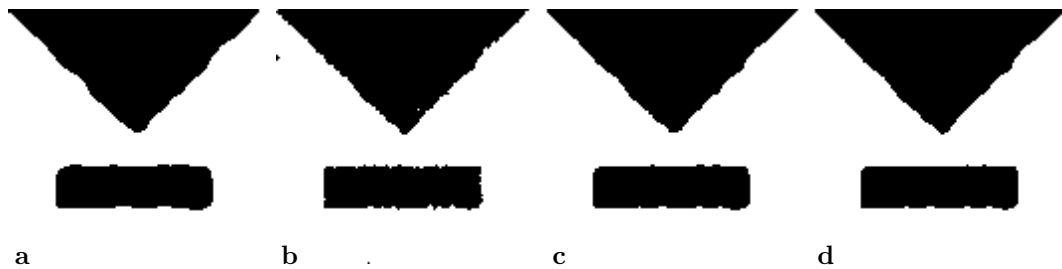
Figure 64: Thresholded versions of the images in Fig. 63

49

the remaining parameters λ and T were estimated autonomously, using the Black–Sapiro's procedure for λ (see [1]), and our decorrelation criterion (2) to determine the optimal T. The values of the parameters employed are shown together with the measured filtering results in Table 21. The filtering performance is evaluated by the MAD distance from the ideal data, so a smaller number means a better result. You can see that in all cases, the nonlinear diffusion filter combined with our time-selection strategy leads to results largely superior to median filter, and slightly better than the recursive filter [3][5]. Several noisy and filtered images can be seen in Figures 65 and 66.

Input image			MAD after filtering			diffusion params.	
Filename	SNR	MAD	median	recursive	diffusion	T	λ
p66n.pgm	48.95	0.45	2.07	0.03	0.76	1.0	8.58
p27n.pgm	31.02	2.41	2.60	2.3	1.76	2.5	8.49
p24n.pgm	28.10	3.21	2.85	3.1	2.05	3.0	8.55
p17n.pgm	19.95	7.32	4.37	5.4	3.20	6.0	26.15
p15n.pgm	17.96	8.97	5.04	5.8	3.55	7.0	26.51
p13n.pgm	14.87	12.33	6.43	6.6	4.24	8.5	35.97
p9n.pgm	9.99	20.84	10.08	8.2	5.93	10.5	77.56
p7n.pgm	8.41	25.10	11.91	8.8	6.79	11.0	119.37
p5n.pgm	6.17	33.62	15.59	10.5	8.38	11.5	192.79
p4n.pgm	4.69	42.14	19.26	13.0	9.99	12.0	284.34

Table 21: The cymbidium experiment. The first three columns give the filename of a given noisy image, the signal-to-noise ratio, and the MAD distance between the original data and the noisy input. The next three columns compare the filtering results of three methods: the 3x3 median filter, the Haindl's recursive filter [3], and the anisotropic NL diffusion. The last two columns present the actually employed diffusion parameters.

---

[5]Except the almost-no-noise case p66n.pgm; this exception was caused by different input data and discretization noise. The results of the recursive filter were kindly provided by Michal Haindl from the Academy of Sciences of the Czech Republic.

Figure 65: The cymbidium experiment. Top: original, noise-free image. Left column (top to bottom): input images p27n.pgm and p17n.pgm. Right column: corresponding images filtered by the anisotropic NL diffusion. The stopping time T was chosen autonomously using the decorrelation criterion; see Table 21 for parameter values and a quantitative evaluation of the filtering performance.

Figure 66: The cymbidium experiment continued. Left column (top to bottom): input images p13n.pgm, p7n.pgm, and p4n.pgm. Right column: corresponding images filtered by the anisotropic NL diffusion. See text and Table 21 for details.

2.13.3 Colour images

The algorithms for NL diffusion and the decorrelation criterion can be easily extended to vector-valued data, including colour images. We present several filtering examples here.

First, Figure 67 shows the effect of the integration scale ϱ on the result of anisotropic diffusion. The results are obtained using the autonomous stopping criterion (2) and it also shows the limitations of that method: although the input image contains no visible corruptions, the high-frequency fur is erroneously considered as noise and oversmoothed in the filtered result. We might advocate the stopping time by saying that the input does not comply well with the piecewise constant assuption implicit in the diffusion equations; anyway, this is an example of a situation where it would be desirable to combine the decorrelation criterion with other information (e.g. the expected amount of noise in the input image) to decide on a better (i.e. earlier) stopping time. Another observation: the filtering result using the decorrelation stopping time (2) is in this case quite stable with respect to the amount of additive noise in the data. This fact is depicted in Figure 68; the main features become apparent in the filtered version and the smoothing may serve as a stabilizing factor for further processing.

2.13.4 Inclined surface

In this section, we present an experiment with piecewise linear data. The ideal signal (image 3d visualized as a surface in three dimensions, where the original grey level is converted to elevation) and the noisy input are drawn at the top of Fig. 69. Such an increasing surface with discontinuities is not easily filtered using classical diffusion filters which are based on the assumption that the data to be filtered are piecewise constant. The image gradient is larger on the sloped surface, and it is rather difficult to tune the parameters of the classical nonlinear diffusion to smooth the noise there without removing the signal discontinuities. Piecewise linear or piecewise increasing data can be recovered better using specialized monotonicity-enhancing diffusion filters, see [5, 6].

The results of two anisotropic NL diffusion filters with autonomous selection of T using the decorrelation criterion can be seen in the bottom row of Figure 69 (the classical one on the left and the monotonicity-enhancing on the right). While the classical filter leads to a rather rough result, trying to approximate the surface with piecewise constant patches, the monotonicity-enhancing procedure is better suited for this kind of data, combines well with the time-selection procedure, and provides a good estimate of the ideal signal.

Figure 67: Top left: input 512×512 image of a baboon. Top right: filtered with anisotropic NL 'edge-enhancing' diffusion ($\varphi_2 = 0.2$); the estimated stopping time was $T = 30$. Center and bottow rows: anisotropic NL diffusion with stronger diffusivity in the coherence direction. The integration parameter ϱ for the computation of the maximum coherence direction was varied (center to bottom and left to right): $\varrho = 0, 3, 5, 10$, and the criterion (2) lead to stopping times $T = 45, 50, 51, 51$, respectively.

Figure 68: Left: baboon with additive Gaussian noise of variance (top to bottom) 30, 50, 100. Right: filtered with anisotropic diffusion using $\varrho = 3$ and autonomous decorrelation time $T = 52, 61, 98$, respectively. The remaining parameters were set as in Figure 67.
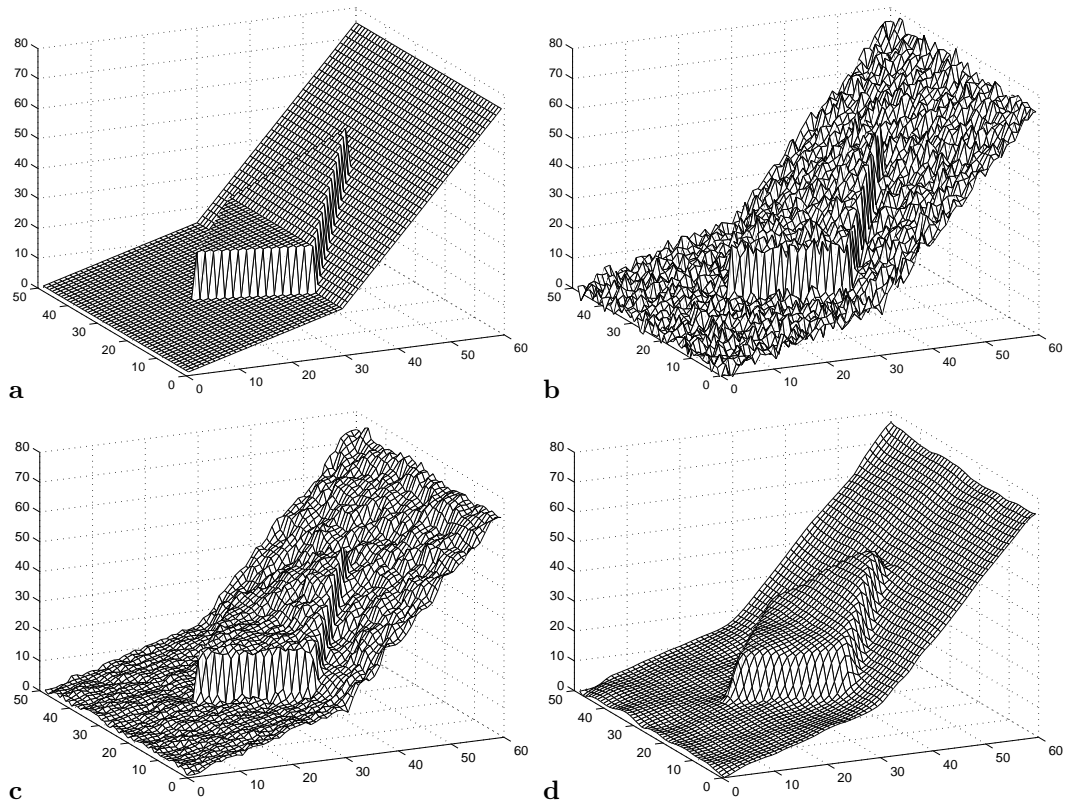
Figure 69: Experiment with two-dimensional data. **(a)** Ideal data. **(b)** Noisy input.
(c) Classical anisotropic NL diffusion, $T = 4$.
(d) Anisotropic NL diffusion for monotonicity enhancement, $T = 10$. In (c)–(d), the stopping time was determined autonomously using the decorrelation criterion.

3   Conclusion

In a previous work [7], we developed a novel method to estimate the optimal stopping time for iterative image restoration techniques such as nonlinear diffusion. The stopping time is chosen so that the correlation of signal $\mathbf{u}(T)$ and 'noise' $\mathbf{u}(0) - \mathbf{u}(T)$ is minimised. This method, which we call *decorrelation criterion* is very general, being based only on the assumption that the noise and the signal in the input image are uncorrelated, and that the filtering method is suitable for that given type of signal; no knowledge on the variance of the noise, and no training images are needed to tune any parameters of the method.

In the current report, we test and validate the performance of that criterion experimentally. Our results suggest that in practical situations with diffusion filters the decorrelation criterion generally provides a good estimate of the optimal stopping time for a wide range of noise levels and filtering parameters. The decorrelation criterion combines best with classical nonlinear diffusion (both isotropic and anisotropic), and with linear diffusion; it is less suitable to estimate the stopping iteration of monotonicity-enhancing diffusion [5], and seems completely unsuitable for iterated median filtering. We have seen that in some cases with NL diffusion, the new criterion outperforms other time selection strategies which use more a priori information e.g. about the noise variance. However, we have also seen situations where our estimation fails, so if more information is available, we would suggest to use it, compute several stopping time estimates using different methods, and compare the results to improve reliability of the estimation.

The minimum of the correlation $|\operatorname{corr}\bigl(\mathbf{u}(0) - \mathbf{u}(t), \mathbf{u}(t)\bigr)|$ can be also used to evaluate the filtering performance of the filter which created the sequence $\mathbf{u}(t)$. This measure can then be used to choose one of several filters which is most suitable for the input data, or to adapt parameters of the diffusion. We have shown some initial experiments in this direction in section 2.12.

References

[1] M. J. Black, G. Sapiro, D. Marimont, and D. Heeger. Robust anisotropic diffusion. *IEEE Transactions on Image Processing*, 7(3):421–432, March 1998.

[2] F. Catté, P.-L. Lions, J.-M. Morel, and T. Coll. Image selective smoothing and edge-detection by nonlinear diffusion. *SIAM Journal on Numerical Analysis*, 29(1):182–193, 1992.

[3] M. Haindl. Recursive square-root filters. In A. Sanfeliu, J. J. Villanueva, M. Vanrell, R. Alquezar, A. K. Jain, and J. Kittler, editors, *Proceedings of the 15th IAPR Int. Conf. on Pattern Recognition*, volume II, pages 1018–1021, Los Alamitos, USA, September 2000. IEEE Computer Society Press.

[4] T. Lindeberg. *Scale-Space Theory in Computer Vision*. Kluwer Academic Publishers, 1994.

[5] P. Mrázek. Monotonicity enhancing nonlinear diffusion. *Journal of Visual Communication and Image Representation*. To appear.

[6] P. Mrázek. *Nonlinear Diffusion for Image Filtering and Monotonicity Enhancement*. PhD thesis, Center for Machine Perception, Department of Cybernetics, Faculty of Electrical Engineering, Czech Technical University, Prague, Czech Republic, 2001.
Available at `ftp://cmp.felk.cvut.cz/pub/cmp/articles/mrazek/Mrazek-phd01.pdf`.

[7] P. Mrázek. Selection of optimal stopping time for nonlinear diffusion filtering. In M. Kerckhove, editor, *Scale-Space and Morphology in Computer Vision. Third International Conference, Scale-Space 2001*, pages 290–298. Springer-Verlag, July 2001.
Available at `ftp://cmp.felk.cvut.cz/pub/cmp/articles/mrazek/Mrazek-scsp01.pdf`.

[8] P. Perona and J. Malik. Scale-space and edge-detection using anisotropic diffusion. *IEEE Transactions on Pattern Analysis and Machine Intelligence*, 12(7):629–639, 1990.

[9] J. Weickert. *Anisotropic Diffusion in Image Processing*. European Consortium for Mathematics in Industry. B. G. Teubner, Stuttgart, 1998.

[10] J. Weickert. Coherence-enhancing diffusion of colour images. *Image and Vision Computing*, 17:201–212, 1999.